

1 Article

# 2 Comparison of catalytic activity of ZIF-8 and Zr/ZIF-8 3 for greener synthesis of chloromethyl ethylene 4 carbonate by CO<sub>2</sub> utilisation

5 Bisi Olaniyan<sup>†</sup> and Basudeb Saha<sup>†\*</sup>

6 School of Engineering, London South Bank University, 103 Borough Road, London SE1 0AA, UK

7 <sup>\*</sup>Corresponding Author: School of Engineering, London South Bank University, 103 Borough Road, London  
8 SE1 0AA. Tel.: +44 (0)20 7815 7190; Fax: +44 (0)20 7815 7699. E-mail address: [b.saha@lsbu.ac.uk](mailto:b.saha@lsbu.ac.uk) (B. Saha).

9 **Abstract:** The catalytic activity of both ZIF-8 and Zr/ZIF-8 has been investigated for the synthesis of  
10 chloromethyl ethylene carbonate (CMEC) using carbon dioxide (CO<sub>2</sub>) and epichlorohydrin (ECH)  
11 under solvent-free conditions. Published results from literature has highlighted the weak thermal,  
12 chemical, and mechanical stability of ZIF-8 catalyst, which has limited its large-scale industrial  
13 applications. The synthesis of novel Zr/ZIF-8 catalyst for cycloaddition reaction of ECH and CO<sub>2</sub> to  
14 produce CMEC has provided a remarkable reinforcement to this weak functionality, which is a  
15 significant contribution to knowledge in the field of green and sustainable engineering. The  
16 enhancement in the catalytic activity of Zr in Zr/ZIF-8 can be attributed to the acidity/basicity  
17 characteristics of the catalyst. The comparison of the catalytic performance of the two catalysts has  
18 been drawn based on the effect of different reaction conditions such as temperature, CO<sub>2</sub> pressure,  
19 catalyst loading, reaction time, stirring speed and catalyst reusability studies. Zr/ZIF-8 has been  
20 assessed as a suitable heterogeneous catalyst outperforming the catalytic activities of ZIF-8 catalyst  
21 with respect to conversion of ECH, selectivity and yield of CMEC. At optimum conditions, the  
22 experimental results for direct synthesis of CMEC agree well with similar literature on Zr/MOF  
23 catalytic performance, where the conversion of ECH, selectivity and the yield of CMEC are 93%,  
24 86% and 76%, respectively.

25 **Keywords:** ECH, epichlorohydrin; CMEC, chloromethyl ethylene carbonate; CO<sub>2</sub>, carbon dioxide;  
26 MOF, metal organic framework; ZIF-8, zeolitic imidazolate framework; Zr/ZIF-8, zirconium/zeolitic  
27 imidazolate framework.

---

## 29 1. Introduction

30 The effective transformation and utilization of anthropogenic carbon dioxide (CO<sub>2</sub>) is a subject  
31 of political and environmental debates in recent years, which have been actively pursued by the  
32 academia and energy industries in order to promote a sustainable environment [1]. The current level  
33 and accumulation of CO<sub>2</sub> in the atmosphere is high and require urgent attention [2]. However,  
34 regardless of environmental regulations and discharge limits placed on greenhouse gases emitted  
35 into the atmosphere, CO<sub>2</sub> is believed to be environmentally benign, abundant, nontoxic, non-  
36 flammable and readily available C1 source for the synthesis of organic carbonate [3]. Therefore, the  
37 synthesis of cyclic organic carbonates *via* the cycloaddition of CO<sub>2</sub> and epoxides is one of the most  
38 promising reaction schemes because of its 100% atom efficiency [4]. Cyclic organic carbonates such  
39 as chloromethyl ethylene carbonate (CMEC), propylene carbonate (PC), styrene carbonate (SC) and  
40 ethylene carbonate (EC) are widely used as polar aprotic solvents, electrolytes for lithium-ion  
41 batteries, automobile, cosmetic, fuel additives materials, alkylating and carbonylating reagents and  
42 fine chemicals for pharmaceuticals [5,6].

43 In the past two decades, several attempts have been made to develop greener and sustainable  
44 catalytic systems for chemical fixation of CO<sub>2</sub>. This includes conventional solid catalysts such as  
45 zeolites, salen Cr(III) complexes, metal oxides, quaternary ammonium salts, polymer-supported

46 catalysts, ionic liquids (ILs) etc. However, these attempts have failed to yield satisfactory results as  
47 most of these catalysts require high temperature and/or pressure (usually around 453 K and pressure  
48 higher than 8 atm), further separation and purification steps and low product yield [7]. This is  
49 uneconomical from a commercial point of view and hence the research has been directed to employ  
50 a novel catalyst that provides solutions to all these shortfalls i.e. metal organic framework (MOF).  
51 Although, microporous materials such as zeolites, crystalline aluminosilicate, activated carbon etc.  
52 have been known for their high surface area and high porosity, however, their applications have been  
53 limited especially in the field of heterogeneous catalysis due to difficulty in pore modification [7].

54 Metal organic framework (MOF) catalysts are identified as multidimensional porous polymetric  
55 crystalline organic-inorganic hybrid materials with exceptional characteristics including ultrahigh  
56 specific surface area, enormous pore spaces and ordered crystalline structure [8]. MOFs have  
57 emerged as a suitable candidate for the synthesis of organic carbonates from CO<sub>2</sub> and epoxide due to  
58 their unique heterogeneity and reusability requirements [9]. MOF-based catalysts often display  
59 higher catalytic activity than their corresponding homogenous catalysts as evidenced in many  
60 catalytic reactions such as ring opening, addition reactions, oxidation reactions, hydrogenation,  
61 isomerization [10]. Zeolitic imidazolate frameworks, (ZIFs), is one of the subclasses of MOFs with a  
62 similar structure to zeolites. It has attractive structural properties and intrinsically lower density.  
63 Many experiments involving ZIF-8 have shown great applications in multidisciplinary fields such as  
64 catalysis, drug deliveries, purification, gas storage [11].

65 Recently, the stability of MOFs for large-scale industrial applications have been questioned in  
66 many published papers [11–16]. This is due to their weak thermal, chemical and mechanical stability  
67 due to the structure of inorganic bricks and the nature of the chemical bonds it forms with the linker  
68 [15]. In order to improve this weak thermal functionality and gain in-depth knowledge of their  
69 catalytic activities, Cavka et al. [15] was the first group to synthesise Zr-based MOFs designated as  
70 zirconium 1,4-dicarboxybenzene, UiO-66 for photocatalysis [17]. The test conducted by the group  
71 found that the increased stability of the Zr-based MOFs is owing to the Zr-O bonds formed between  
72 the cluster and carboxylate ligands [18]. Several other groups have thereafter explored this  
73 opportunity, which has seen increased in the application of Zr-based MOFs in many research  
74 activities. Demir et al. [19] utilized UiO (University of Oslo) type zirconium metal-organic  
75 frameworks in a solvent-free coupling reaction of CO<sub>2</sub> and ECH for the synthesis of epichlorohydrin  
76 carbonate (ECHC). The results of their experiments have increased the use of Zirconium-based (Zr-  
77 based) MOFs for the catalytic synthesis of organic carbonates from CO<sub>2</sub> and epoxides.

78 From our experiments, the synthesis of Zr-doped MOF (Zr/ZIF-8) for the cycloaddition reaction  
79 of CO<sub>2</sub> and ECH in the synthesis of chloromethyl ethylene carbonate (CMEC) has demonstrated  
80 reasonable thermal stability under relatively mild reaction conditions without using any solvent or  
81 co-catalyst. Although, the syntheses of several Zr-based MOFs have been reported in recent times  
82 (albeit in early stages), only a few were employed for catalytic studies even more rarely for the  
83 synthesis of organic carbonates from CO<sub>2</sub> and epoxides. Zr-based MOFs have exhibited increased  
84 structural tailorability as a result of the organic linkers in the catalyst frameworks [8].

85 Zirconium based MOFs have demonstrated proof-of-concept applications in several areas such  
86 as toxic analyte, catalysis, gas storage, *vivo* drug delivery and bio-sensing [10]. In this paper, a novel  
87 Zr/ZIF-8 has been successfully synthesised using conventional solvothermal method. The prepared  
88 catalyst has been assessed as an innovative greener and sustainable heterogeneous catalyst for the  
89 direct synthesis of chloromethyl ethylene carbonate from carbon dioxide and epichlorohydrin. The  
90 effect of various reaction parameters has been investigated and critically analysed. These include the  
91 effect of reaction time, catalyst loading, temperature, CO<sub>2</sub> pressure and stirring speed. Catalyst  
92 reusability studies of Zr/ZIF-8 was also investigated to establish its stability and reusability for the  
93 synthesis of CMEC.

94  
95  
96  
97

## 98 2. Experimental methods

### 99 2.1. Chemicals and materials

100 Acetone (99%), chloromethyl ethylene carbonate (99 %), epichlorohydrin (purity; 99%), zinc  
101 nitrate hexahydrate ( $\text{Zn}(\text{NO}_3)_2 \cdot 6\text{H}_2\text{O}$  (purity; 99%), dimethylformamide (purity; 99%) and zirconium  
102 (IV) oxynitrate hydrate ( $\text{ZrO}(\text{NO}_3)_2 \cdot 6\text{H}_2\text{O}$ , 99.99%) were purchased from Sigma-Aldrich Co. LLC.  
103 Methanol (99%) and *n*-pentane 99.8%) were both procured from Fisher Scientific UK Ltd. ZIF-8  
104 catalyst was purchased from Sigma-Aldrich Co. LLC under the trademark of Basolite Z1200. All  
105 chemicals and catalysts were used without further purification or pre-treatment.

### 106 2.2. Catalysts preparation

107 Preparation of ZIF-8 and zirconium-doped ZIF-8 (Zr/ZIF-8) were synthesized according to a  
108 method, which was previously described elsewhere [20,21]. Briefly, 8 mmol of zinc nitrate  
109 hexahydrate ( $\text{Zn}(\text{NO}_3)_2 \cdot 6\text{H}_2\text{O}$  99.99%) and zirconium (IV) oxynitrate hydrate ( $\text{ZrO}(\text{NO}_3)_2 \cdot 6\text{H}_2\text{O}$ ,  
110 99.99%) solutions in a stoichiometric ratio of Zn:Zr = 10:0 and Zr:Zn =9:1 (to synthesis ZIF-8 and  
111 Zr/ZIF-8 respectively) were dissolved in 6.2 mmol of methanol. A separate solution of 14.2 mmol of  
112 2-methylimidazole and 600 ml of methanol was prepared in another flask, which was added by  
113 dropwise addition to the Zr-Zn based solution. The mixture conducted in an ambient temperature  
114 under nitrogen flow was vigorously stirred for 6 hrs. The Zr-doped ZIF-8 crystals were collected and  
115 separated by centrifugation at 300 rpm for 30 min. The solution was washed thoroughly with  
116 methanol three times and then dried at room temperature conditions. The crystals were left to dry  
117 overnight at 373 K. The greyish-white powders of Zr-ZIF-8 samples were further washed with DMF  
118 for 24 h in order to remove any excess of an unreacted organic linker. The solution was then heated  
119 at a temperature of 373 K in order to activate it. The samples were allowed to cool to room  
120 temperature naturally before been capped in a vial and refrigerated, ready for use in catalytic  
121 reactions. The obtained samples were identified with a stoichiometric ratio of Zr:Zn =10:0 and Zr:Zn  
122 = 1:9 for ZIF-8 and Zr/ZIF-8 respectively.

### 123 2.3. Experimental procedure for the synthesis of chloromethyl ethylene carbonate (CMEC)

124 In a typical cycloaddition reaction, a 25 mL stainless steel high-pressure reactor was initially  
125 charged with a specific amount of Zr/ZIF-8 catalyst and the limiting reactant, epichlorohydrin. A  
126 desired temperature was set on the reactor's panel controller; the reactor was then sealed and stirred  
127 continuously at a known stirring speed. At the desired temperature, a specific amount of liquid  $\text{CO}_2$   
128 was charged through a supercritical fluid (SCF) pump into the reactor. The reaction was left for the  
129 desired reaction time. After the reaction was completed, the reactor was cooled down to room  
130 temperature and the mixture was collected and filtered. The catalyst was separated, washed with  
131 acetone and dried in a vacuum oven. A known amount of methanol (used as internal standard) was  
132 added to the product and analysed using a gas chromatograph (GC). The effect of different reaction  
133 parameters was investigated. These include catalyst loading, stirring speed,  $\text{CO}_2$  pressure,  
134 temperature and reaction time. Reusability studies of both catalysts were also carried out in order to  
135 investigate the stability of the catalysts for the synthesis of chloromethyl ethylene carbonate.

### 136 2.4 Method of analysis

137 A specific quantity of internal standard, methanol added to a known sample of the product was  
138 analyzed using a Gas Chromatography (GC) (Model: Shimadzu GC-2014). The stationary phase was  
139 a capillary column with dimensions (30 m length, 320  $\mu\text{m}$  inner diameter and 0.25  $\mu\text{m}$  film thickness).  
140 Oxygen (99.9%) and hydrogen (99.9%) were used as ignition gases. The carrier gas used for the mobile  
141 phase was a high purity helium (99.9%) with a flow rate maintained at 1  $\text{mL min}^{-1}$ . A temperature  
142 program was developed for the system where both the injector port and detector temperatures were  
143 kept isothermally at 523 K. Other selected program includes split ratio of 50:1 and injection volume  
144 of 0.5  $\mu\text{L}$ . The column temperature was initially maintained at 323 K for 5 min then followed by a

145 temperature ramp at a flow rate of 50 K min<sup>-1</sup> to a temperature of 523 K with a 12 min run for each  
 146 subsequent samples. The chromatogram shows that ECH peak at ~3.5 min, methanol at ~3.8 min  
 147 CMEC at ~11 min.

### 148 2.5. Proposed reaction mechanism

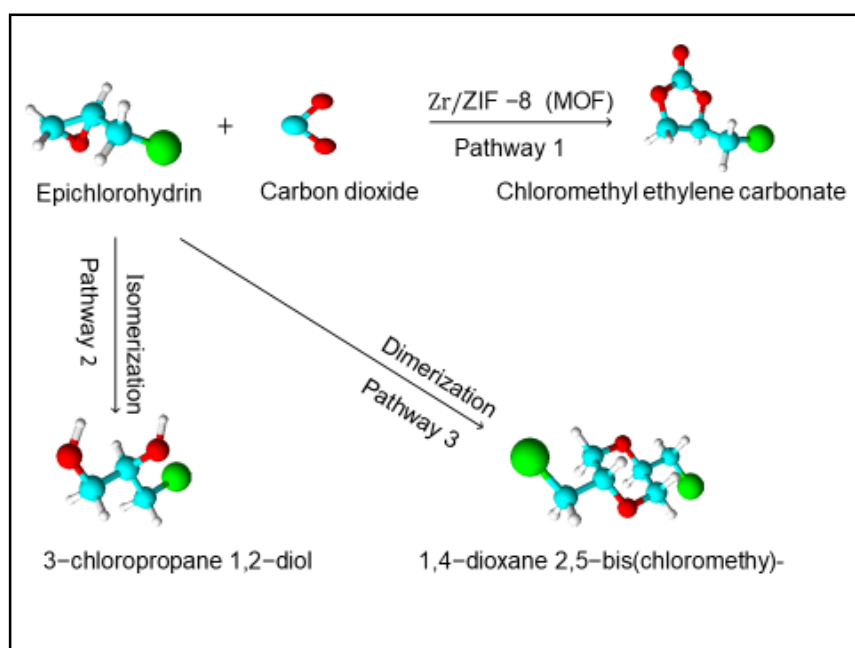
149 The proposed reaction mechanism involves two steps:

150

- 151 ▪ The ring-opening of epoxides by a catalyst;
- 152 ▪ Incorporation of carbon dioxide into the opening to form the cyclic carbonate.

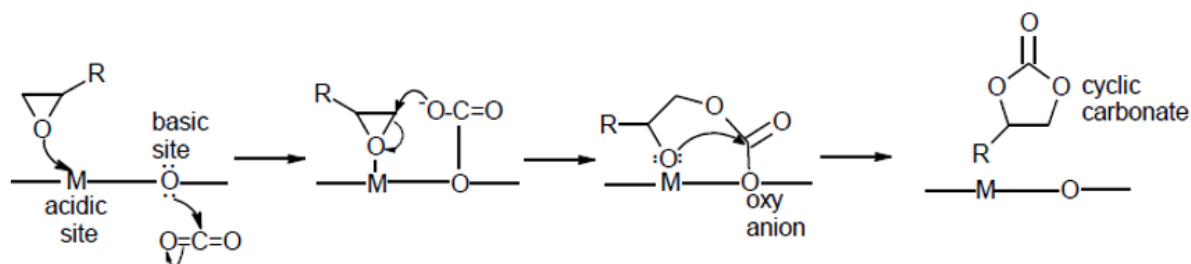
153

154 The coupling reaction of CO<sub>2</sub> with epoxides can be initiated by activating either the epoxide or  
 155 CO<sub>2</sub> or both at the same time [22]. This reaction, using a suitable heterogeneous catalyst produces  
 156 desired organic carbonates along with other side products. Figure 1 shows reaction pathways 1, 2  
 157 and 3 with corresponding products being chloromethyl ethylene carbonate, 3-chloropropane 1,2-diol  
 158 and 2,5-bis (chloromethyl)-1,4-dioxane respectively. The epoxide is activated when the oxygen atom  
 159 interacts with the Lewis acid, this is then followed by a nucleophilic attack that provokes the opening  
 160 of the epoxide ring [23] as shown in Figure 2. The activation of CO<sub>2</sub> can occur both through a  
 161 nucleophilic attack with the oxygen atom as a nucleophile or an electrophilic attack with the carbon  
 162 atom as an electrophile [24]. Figure 2 shows a proposed reaction mechanism for the synthesis of  
 163 CMEC, where R is an alkyl group, A is a metal atom with a Lewis acid site while B is an oxygen atom  
 164 with a Lewis basic site. Zr/ZIF-8 is a dual-functional catalyst, which contains both the acidic and basic  
 165 sites that are associated with the Lewis acid Zn<sup>2+</sup> ions and the basic imidazole groups, respectively.  
 166 The by-products identified with the coupling reaction of CO<sub>2</sub> and ECH as identified by the GC  
 167 analysis are 3-chloropropane 1,2-diol and 2,5-bis (chloromethyl)-1,4-dioxane (see Figure 1).



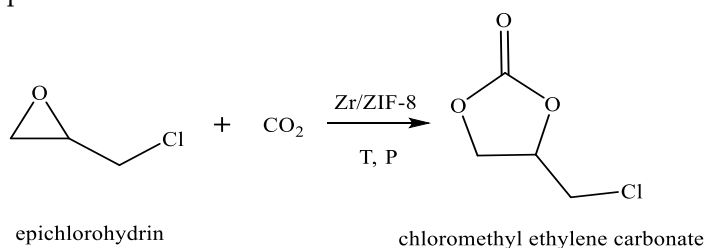
168

169 **Figure 1.** Reaction pathways for cycloaddition reaction of ECH and CO<sub>2</sub>.



170  
171 **R** is an alkyl group, **M** is a metal atom (acidic site) and **O** is oxygen atom (basic site)  
172

173 **Figure 2.** Proposed reaction mechanism for the cycloaddition reaction of CO<sub>2</sub> to ECH over an acid-  
174 base pairs.



175  
176  
177 **Figure 3.** Schematic representation of ECH-CO<sub>2</sub> cycloaddition reaction.

## 178 2.6. Catalyst characterization

179 The powder X-ray diffraction (XRD) patterns of the samples was analysed at room temperature  
180 with a characteristics peaks range of  $5 < 2\theta < 35$  at a scanning rate of  $0.5^\circ\text{min}^{-1}$ . The catalyst was placed  
181 on a zero-background silicon sample holder using a Bruker D8 Advance x-ray diffractometer in  
182 transmission geometry with CuK $\alpha$  radiation ( $\lambda = 1.5406^\circ \text{ \AA}$ ) at 40 kV and 40 mA. The samples were  
183 slightly grinded before measurements were taken so as to prevent preferential orientation of  
184 individual crystals during sample analysis.

185 The Brunauer-Emmett-Teller (BET) surface area of the as-prepared catalyst was analysed with a  
186 Micromeritics Gemini VII analyser at room temperature (291 K). Prior to BET analysis, the samples  
187 were degreased in a turbomolecular pump vacuum at 423 K for 8 h. The surface area and nitrogen  
188 adsorption/desorption isotherm measurements were taken at liquid nitrogen temperature of 77 K  
189 (purge gas supplied by BOC, UK). In order to achieve greater degree of accuracy in the accumulation  
190 of the adsorption data, the Micromeritics Gemini analyser was fitted with pressure transducers to  
191 cover the range of 133 Pa, 1.33 kPa and 133 kPa.

192 The Fourier transform infrared (FTIR) spectra ( $4500\text{-}600\text{ cm}^{-1}$ ) of the samples were obtained using  
193 Nicolet Magna-IR 830 spectrometer in KBr disks at room temperature with a resolution of  $2\text{ cm}^{-1}$ . The  
194 specimen was mixed KBr in ratio 1:300, the mixture was ground in an agate mortar to a very fine  
195 powder. The product was oven dried for 12 h at 373 K, 250 mg of the dry samples were used to make  
196 a pallet; the pallet was analysed, and the spectra were recorded by 32 scans with  $4\text{ cm}^{-1}$ .

197 Particle size morphologies and microstructures of the as-synthesised Zr/ZIF-8 catalyst was  
198 examined using JEOL JSM-35C instrument operated at voltage 20 kV acceleration. Prior to imaging,  
199 the specimen was carbon-coated (5-10 nm) under a vacuum condition using Emitech K550X sputter  
200 coater, this was done to enhance material conductivity. The particle mean size of the specimen were  
201 calculated by taking a manual measurement of about 300 crystals in the SEM images using the field-  
202 emission scanning electron microscope (FE-SEM). FE-SEM spectra produced were used to examine  
203 the particle size and morphology.

204 Transmission electron microscopy (TEM) images of the catalyst were examined using a high  
205 resolution TEM (HRTEM)). A sample of the specimen were sonicated in ethanol for 15 min and was  
206 then placed by a dropwise onto a carbon film-supported copper grid. The as-prepared sample was  
207 allowed to dry at room temperature before inserting into a sample holder. X-ray photoelectron

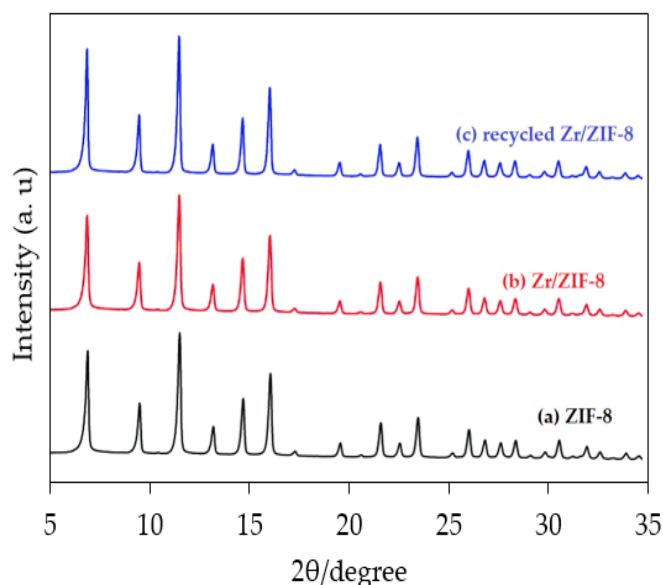
208 spectroscopy (XPS) of the samples was recorded on krato axis ultra DLD photoelectron spectrometer,  
 209 a surface science instrument SSx-100 using a monochromatic Al KR X-ray source operating at 144 W.  
 210 Raman spectroscopy measurements of the specimen were taken at room temperature with Horiba  
 211 Jobin Yvon LabRAM spectrometer equipped with aHeNe laser operating at a wavelength of 633 nm  
 212 ( $E_{ex}=1.96\text{eV}$ ) and Coherent Innova 70 ion laser at a wavelength of 458 nm, 488 nm and 514 nm.

### 213 3. Results and Discussion:

#### 214 3.1. Catalyst characterisation

215 The X-ray diffraction patterns of ZIF-8, Zr/ZIF-8 and recycled Zr/ZIF-8 are shown in Figure 4.  
 216 The diffraction peaks appeared at small  $2\theta$  angles with eight diffraction peaks at 7.31, 10.31, 12.71,  
 217 14.71, 16.41, 18.01, 24.61, and 26.71 which are indexed to the (011), (002), (112), (022), (013), (222), (233),  
 218 and (134) planes, respectively. The XRD patterns of both Zr/ZIF-8 and recycled Zr/ZIF-8 catalysts are  
 219 identical as shown in Figure 4, confirming that Zr/ZIF-8 has high crystal stability under the normal  
 220 reaction conditions. These results are in agreement with simulated patterns reported in other  
 221 literature [24,25,26]. The decrease in peak intensity of these diffractions was also observed at ( $2\theta =$   
 222  $28-35^\circ$ ) indicating the effect of excess doping of Zr into ZIF-8 framework. A similar phenomenon was  
 223 reported by Schejn et al. [20]. The XRD pattern of Zr/ZIF-8 also show a characteristic peak of ZIF-8  
 224 with no diffraction peak of zirconium nitrate, a similar observation was reported elsewhere by Thi et  
 225 al. [21].

226 Although, the peak intensity of Zr/ZIF-8 may be slightly lower when compared to commercial  
 227 Basolite Z1200, purchased from Sigma Aldrich. Nevertheless, the experiments of Nordin et al. (2014)  
 228 [28] establishes that guest molecules (such as zirconium) occupying MOF pore spaces may cause  
 229 pattern destructive and subsequently, a retarded gas uptake capacity in the MOF. A further and in-  
 230 depth examination of the XRD patterns of the specimen beyond this study could reveal some  
 231 surprising details as doping of zirconium into ZIF-8 could enlarge its pore spaces [29] thereby  
 232 inducing a crystallographic defect in the Zr/ZIF-8 catalyst.  
 233



234  
 235

236 **Figure 4.** X-ray diffraction (XRD) patterns of (a) ZIF-8, (b) Zr/ZIF-8 and (c) recycled Zr/ZIF-8 catalysts  
 237

238 The Nitrogen adsorption-desorption isotherms of ZIF-8, Zr/ZIF-8 and the recycled Zr/ZIF-8  
 239 catalysts are shown in Figure 5. The samples were measured at liquid temperature of 77k at 373 K for  
 240 24 h. The three isotherms showed an attribute of a microporous framework with a sharp hysteresis  
 241 loop of P/P<sub>0</sub> between 0.8 and 1.0. However, the pristine ZIF-8 catalyst demonstrates a typical type-I  
 242 isotherm behaviour [30]. While Zr/ZIF-8 and the recycled Zr/ZIF-8 catalysts both shows typical type-

243 IV isotherms with a type H<sub>4</sub> hysteresis loop in the range of P/P<sub>0</sub> = 0.4–0.8 indicating the presence of  
 244 mesopores [31]. Meanwhile, an increase in the volume adsorbed at low relative pressure is consistent  
 245 with interparticle voids, which is indicative of dual macro-mesoporosity of Zr/ZIF-8 lattice according  
 246 to IUPAC classification [31–33].

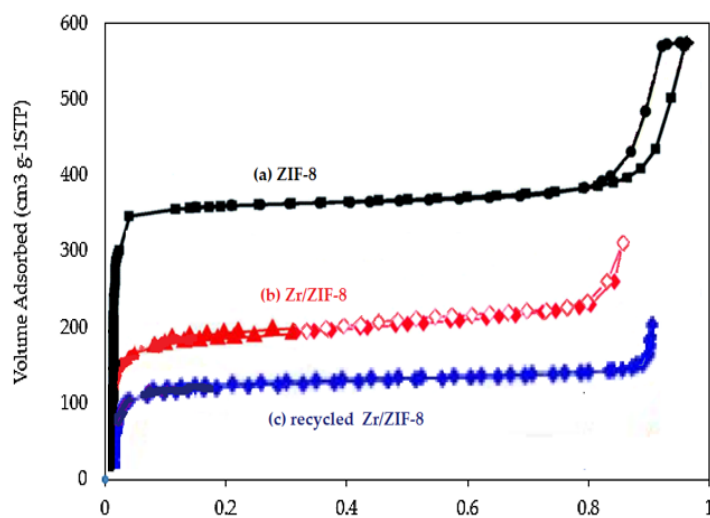
247 The specific BET surface area ( $S_{\text{BET}}$ ) of the catalysts have been calculated using BET equation.  
 248 The pore size distribution was derived from the nonlinear density functional theory (DFT) model  
 249 (calculated using computer software). The surface area and micropore volume of Zr/ZIF-8 was  
 250 generally lower than ZIF-8 as shown in table 1. The lower BET surface area and pore volume of  
 251 Zr/ZIF-8 may be caused by the blockage of the pore cavities of host molecule as a result of deposition  
 252 of zirconium particles in the ZIF-8 shell, a phenomenon that has been previously reported by Rai et  
 253 al. [34]. Surprisingly, the total pore volume and the BET specific surface area of recycled Zr/ZIF-8  
 254 catalyst had both decreased after the reaction. This observation may be attributed to agglomeration  
 255 of coke deposits in the pore spaces, resulting in the blockage of some micropores and mesopores.  
 256 [36].

257 These results reflect a good pore size distribution of the samples microporous network [34, 37].  
 258 Although, variation may exist in particles BET surface area and pore volume from one literature to  
 259 another, this may be attributed to post-synthesis work-up procedures such as further purification  
 260 processes and activation of MOF samples [39]. The BET surface area as shown in Figure 5 are in  
 261 agreement with previous literature [41].  
 262  
 263

264 **Table 1.** Comparison of BET, pore-volume, and pore size for ZIF-8 and Zr/ZIF-8 crystals  
 265

Entry	Material	$S_{\text{BET}}$ ( $\text{m}^2\text{g}^{-1}$ )	Pore volume ( $\text{cm}^3\text{g}^{-1}$ )	Pore size (nm)
1	ZIF-8	1700	0.664	1.30
2	Zr/ZIF-8	1458	0.536	1.23
3	Zr/ZIF-8 (recycled)	1378	0.498	1.21

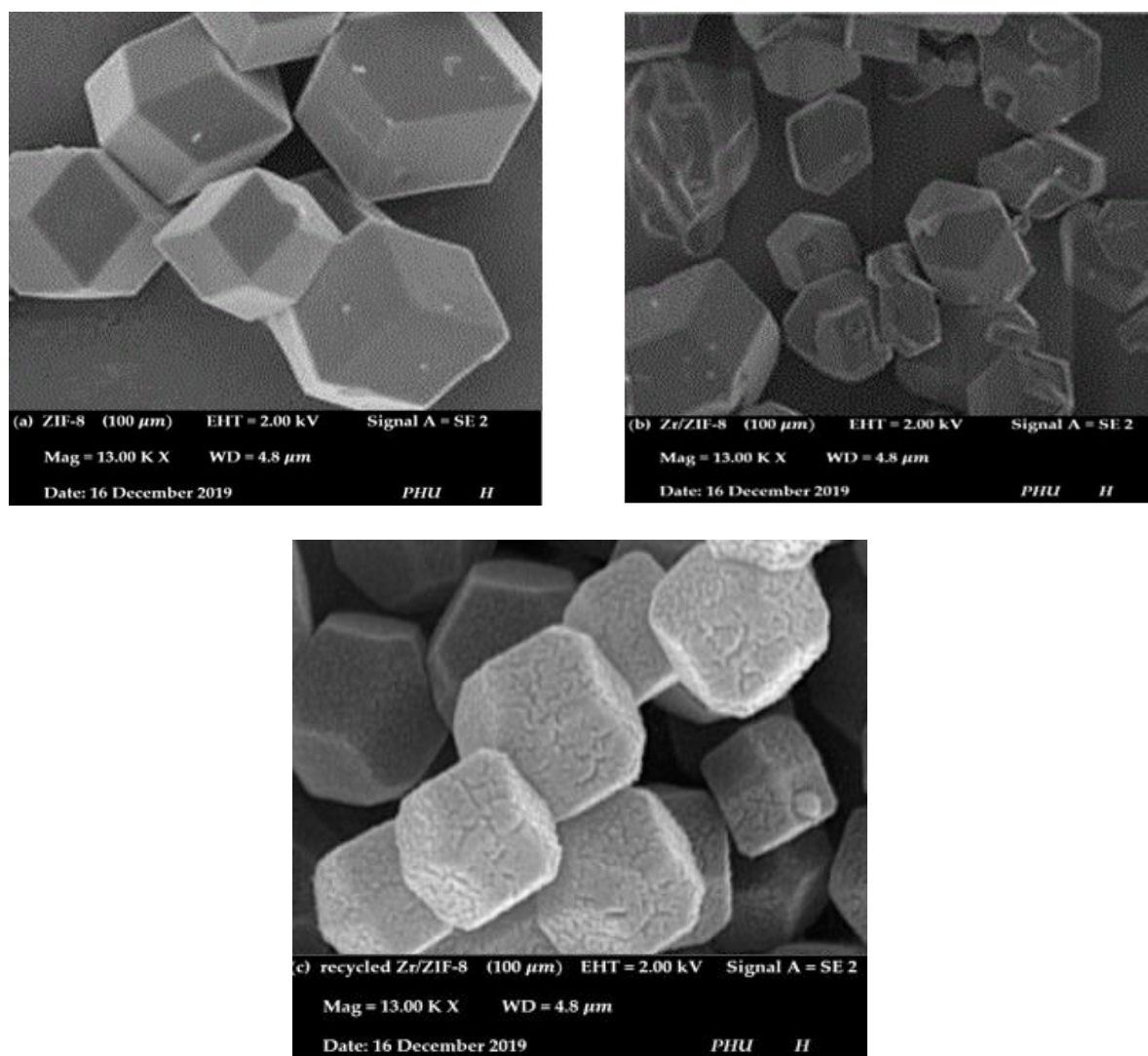
266  
 267



268  
 269  
 270  
 271

**Figure 5.** N<sub>2</sub> adsorption-desorption isotherms of (a) ZIF-8 (b) Zr/ZIF-8 and (c) recycled Zr/ZIF-8 synthesized with 10% dopant of Zr.

272 Figure 6 shows the morphologies and microstructures of ZIF-8, fresh and recycled Zr/ZIF-8  
 273 catalysts using the scanning electron microscope (SEM) with an average particle size diameter of  
 274 100 $\mu$ m. Figure 6a shows an evolution of ZIF-8 crystal from cubes with 6 faces [100] to intermediates  
 275 shapes, and finally to a more stable equilibrium rhombic dodecahedral shape with edges exposing  
 276 12 faces [110] [40]. Figure 6b (Zr/ZIF-8) revealed very slight morphological alterations to Figure 6a  
 277 (ZIF-8) framework. The slight alterations are a genuine indication of a stable Zr/ZIF-8 catalyst  
 278 comparing to the report of Yin et al. [41]. Furthermore, the hexagonal shape of the recycled catalyst  
 279 in Figure 6c showed a very small change after the cycloaddition reaction. A close examination of the  
 280 SEM images of Figure 6a and Figure 6b shows no significant effect of attrition on the overall particle  
 281 aggregation between the two structures. The SEM image of recycled Zr/ZIF-8 in Figure 6c showed  
 282 rather small isolated monodispersed particles with a well-defined truncated rhombic dodecahedron  
 283 structure caused by the presence of dopant in the host molecule. Essentially, the SEM images of the  
 284 samples are consistent with the XRD results in Figure 4 and the thermal stability of Zr/ZIF-8 as shown  
 285 in Figure 17 of the catalyst reusability studies. It is worth mentioning that, the increased average  
 286 crystal size of recycled Zr/ZIF-8 catalyst in the range of ~100–170 nm (Figure 6c) may be attributed to  
 287 Ostwald ripening and/or recrystallization effect [42]. A phenomenon which explains a possible  
 288 increase in the average crystal size of the reused catalyst during cycloaddition reaction, especially at  
 289 a higher temperature (reaction temperature 353 K).  
 290

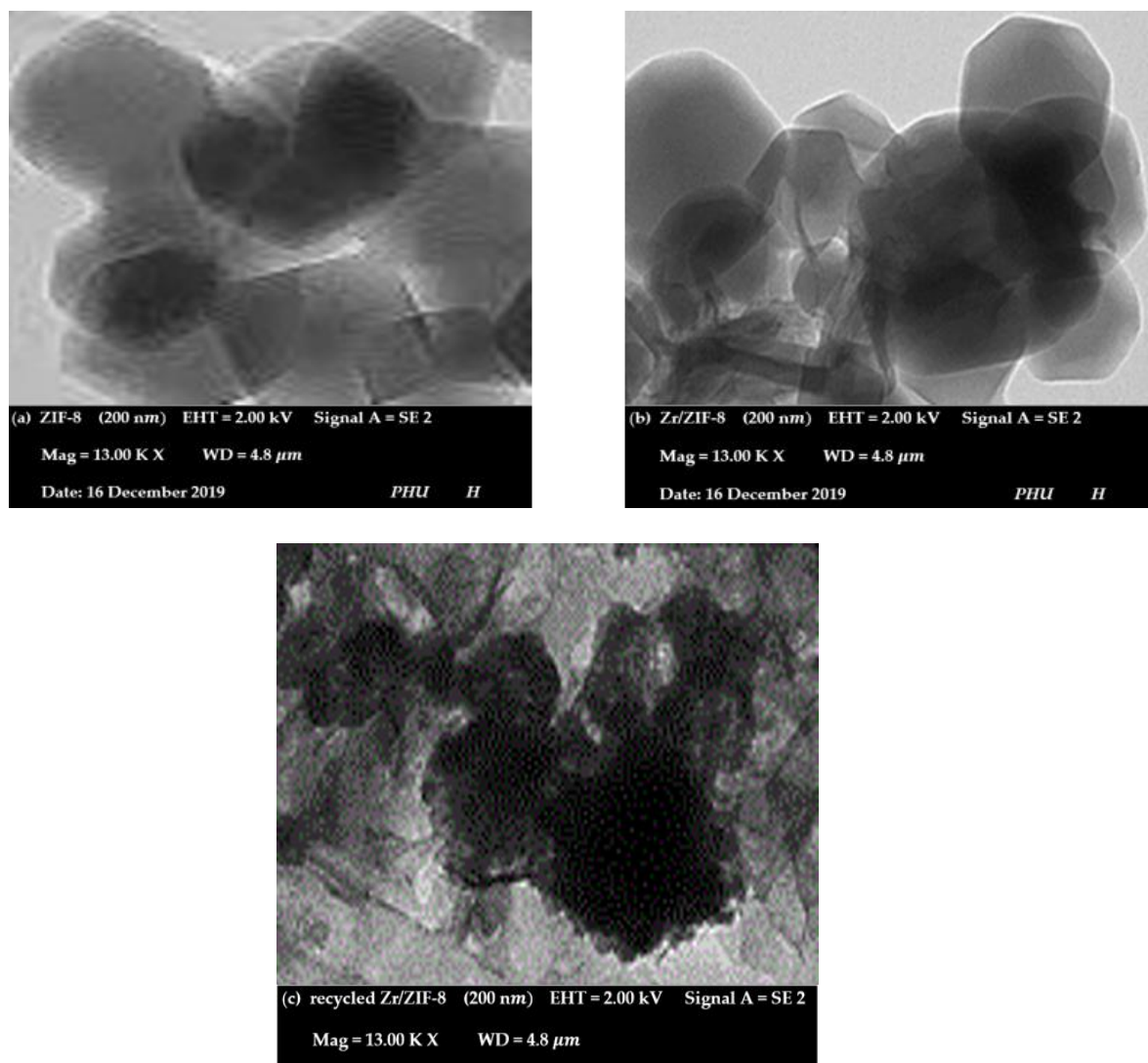


291  
 292

293  
 294  
 295  
 296

**Figure 6.** SEM images of (a) ZIF-8 crystals, (b) Zr/ZIF-8 and (c) recycled Zr/ZIF-8 crystals synthesized with 10% dopant of Zr

297 A low-magnification TEM images of the samples were carried out in order to examine the  
 298 structural changes taking place on the surface of the samples. Figure 7a and 7b showed well-shaped  
 299 high-quality homogenous crystals with a remarkable rhombic dodecahedral shape and average  
 300 crystal size of about 100  $\mu\text{m}$  which conforms to earlier literature [42]. It can be observed from the  
 301 image in Figure b that there are no obvious aggregations or changes in particle size and morphology  
 302 from Figure 7a. The TEM image of the recycled catalyst (Figure 7c) shows that the catalyst crystals  
 303 were highly stable during the cycloaddition reaction of  $\text{CO}_2$  and ECH.  
 304  
 305



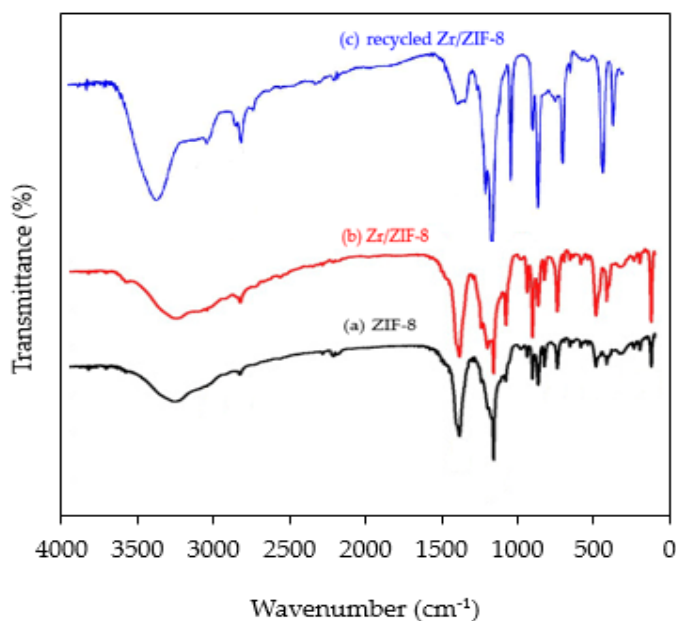
306  
 307

308  
 309

310 **Figure 7.** Transmission Electron Microscopy (TEM) image of (a) pristine ZIF-8 crystals (b) Zr/ZIF-8  
 311 and (c) recycled Zr/ZIF-8 synthesized with 10% dopant of Zr  
 312

313 Figure 8 shows the FT-IR spectra of ZIF-8, Zr/ZIF-8 and the recycled Zr/ZIF-8 with an absorption  
 314 region of 500–4000  $\text{cm}^{-1}$ . The three samples show several bands with no substantial difference in the  
 315 spectra. For example, a typical adsorption band at 423  $\text{cm}^{-1}$  is attributed to the Zn-N bond vibrations  
 316 indicating that zinc molecules of the imidazole ring are well-knitted during the reaction to nitrogen  
 317 atoms in 2-methylimidazolate (2-Hmim) linkers to form the ZIF frameworks [43]. The absorption  
 318 spectra at 2926  $\text{cm}^{-1}$  can be ascribed to the aromatic moieties, while the spectra at 3133  $\text{cm}^{-1}$  can be  
 319 attributed to the aliphatic imidazole ring due to C-H stretching [44]. The missing adsorption spectra  
 320 in the region of 3400 to 2200  $\text{cm}^{-1}$  is a strong indication of a fully deprotonated imidazole ring during  
 321 the formation of the ZIF-8 frameworks [45]. The strong sharp peak at 1449  $\text{cm}^{-1}$  can be assigned to

322 the C–C bonding in the benzene ring. The peak at  $1579\text{ cm}^{-1}$  can be attributed to C = N vibrations  
 323 mode [45]. While the spectra in the band range between  $1100$  and  $400\text{ cm}^{-1}$  can be assigned to C-N  
 324 stretching vibrations. The small peaks at  $1245$  and  $1255$  can be assigned to C-N and C≡N groups  
 325 respectively indicating the presence of imidazole molecules in the samples frameworks. The Zr-N  
 326 bonding vibration located between  $550$  and  $620\text{ cm}^{-1}$  in Zr/ZIF-8 catalyst [46]. All characteristic peaks  
 327 of ZIF-8 can be observed both in Zr/ZIF-8 and the recycled Zr/ZIF-8, indicating a successful  
 328 combination and interaction between Zr and ZIF-8. This observation is a strong indication that the  
 329 frameworks of ZIF-8 have not been affected after the incorporation of Zr. This results in agreement  
 330 with the report of Giraldo et al. [47] experiments.  
 331

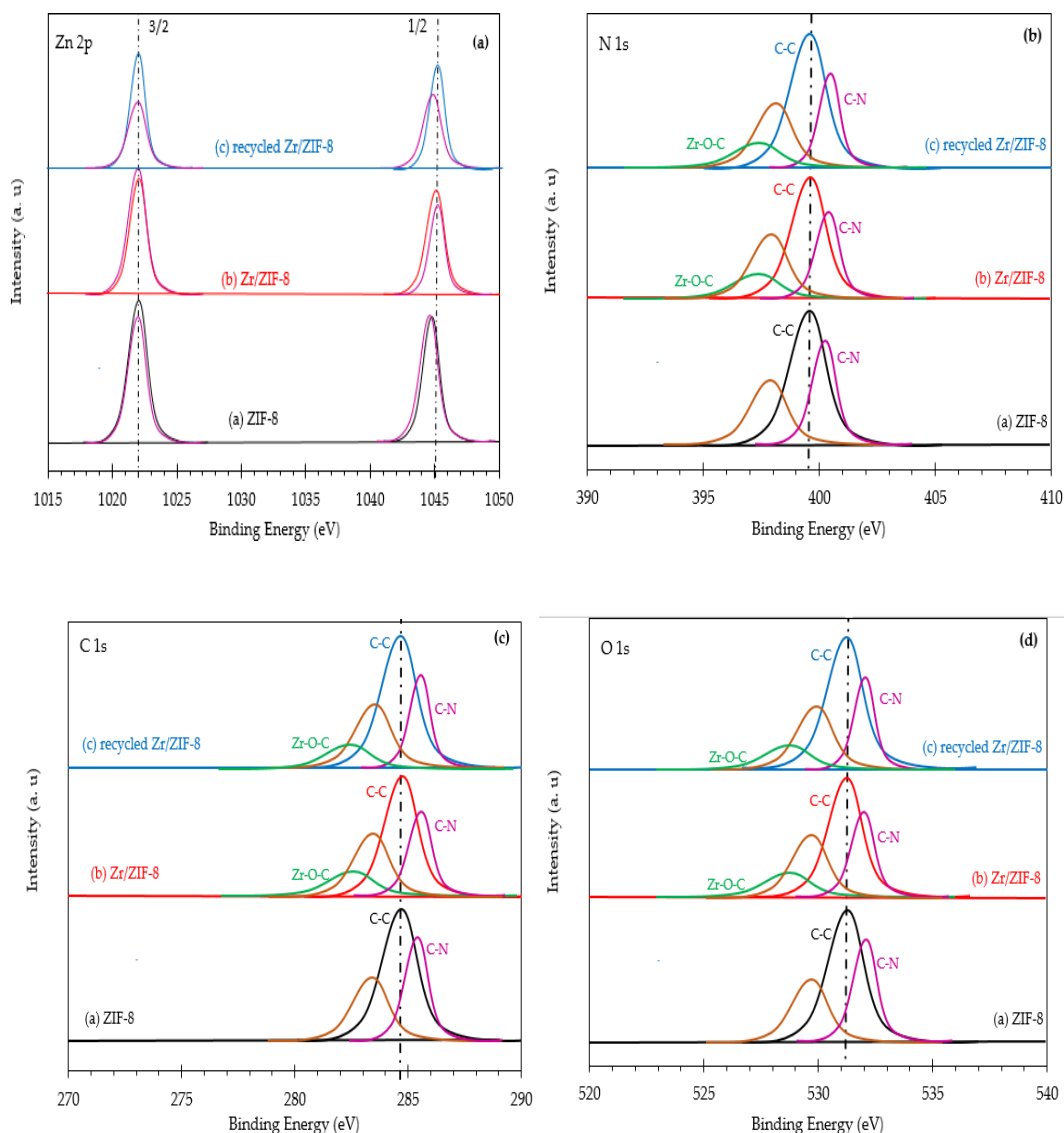


332  
 333 **Figure 8.** FTIR spectra of (a) ZIF-8, (b) Zr/ZIF-8 and recycled Zr/ZIF-8 particles  
 334

335 The X-ray photoelectron spectroscopy (XPS) spectra in Figure 9 clearly shows the chemical state  
 336 of the element present in pristine ZIF-8 frameworks (Zn, C, N) and O, while those elements present  
 337 in Zr/ZIF-8 sample include Zn, C, N, O and Zr species. Figure 9a exhibits high resolution XPS  
 338 spectra showing two strong peaks with binding energy of  $1044.3\text{ eV}$  and  $1021.1\text{ eV}$  which can be  
 339 assigned to Zn  $2p^{1/2}$  and Zn  $2p^{3/2}$  components, respectively confirming the presence of Zn (II) ions  
 340 attached with nitrogen in the imidazole ring [36]. This result is consistent with the XRD result as  
 341 shown in Figure 4. With the incorporation of Zr into ZIF-8, the binding energy of Zn  $2p^{1/2}$  and  $2p^{3/2}$   
 342 have slightly increased, this could be as a result of the chemical environment of zinc and the  
 343 interaction between zinc and zirconium. All spectra have been normalized to the magnitude of the  
 344 Zn  $2p^{3/2}$  and Zn  $2p^{1/2}$  peaks, so that changes in intensity are relative to the amount of Zn in the surface  
 345 region. Similarly, Figure 9b shows high-resolution N1s spectra of all samples. The N1s spectra can be  
 346 deconvoluted into three characteristic peaks found at  $399.0$  and  $399.8$  and  $398\text{ eV}$  which can be  
 347 assigned to the pyridinic, pyrrolic, and graphitic, respectively. These can be related to the N species  
 348 of 2-methyl imidazole ring [35]. C1s spectra shows four different characteristic peaks corresponding  
 349 to C–C at  $284.1\text{ eV}$ , C–N at  $285.8\text{ eV}$ , C–O at  $286.4\text{ eV}$  all assigned to 2-methyl imidazole ring [48].  
 350 The low peak found at  $283.4\text{ eV}$  could be as a result of Zr doping into ZIF-8 frameworks [49]. Figure 9d  
 351 shows high resolution O1s spectra that has been deconvoluted into two characteristic peaks with  
 352 binding energy  $532.3$  and  $531.8\text{ eV}$  correspond to  $\text{O}^{2-}$  found in Zn-O bonding and carboxylate species,  
 353 respectively [36]. The relatively low peak intensity of Zr –O in O1s, C1s and N1s is a strong indication  
 354 that the ZIF-8 frameworks are not affected by the presence of dopant, which perfectly agreed with  
 355 the result of Mao et al. [49].

356

357

358  
359  
360361  
362

**Figure 9.** X-ray photoelectron spectroscopy (XPS) spectra showing deconvoluted regions of ZIF-8, Zr/ZIF-8 catalyst and recycled Zr/ZIF-8 catalysts. (a) Zn 2p (b) N 1s (c) C 1s (d) O 1s

365

366

367

368

369

370

371

372

373

374

375

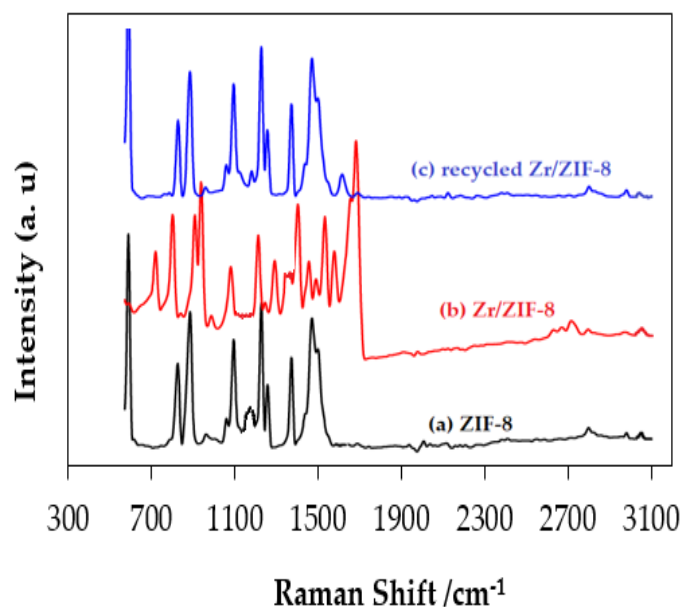
376

377

378

Raman spectra of ZIF-8, Zr/ZIF-8 and the recycled Zr/ZIF-8 were observed using a Renishaw Ramascope 1000 (model: 52699). Figure 10 shows that Zr/ZIF-8 exhibited several Raman spectra at the following peaks 687, 892, 1149, 1186, 1462, 1568, 2931, 3114 and 3131  $\text{cm}^{-1}$  similar to ZIF-8 spectra. The spectra at 1116 and 1484  $\text{cm}^{-1}$  corresponding to bands D and G, respectively found in the Raman spectrum of ZIF-8 [50], have not been observed in the Zr/ZIF-8 and the recycled Zr/ZIF-8 spectra. This may be as a result of a split of the main bands at 1143 and 1508  $\text{cm}^{-1}$  as previously reported by Biswal et al. [51]. The spectra found at 278  $\text{cm}^{-1}$  may be attributed to Zn–N stretching, while the spectra at 683, 1143, 1456, and 1508  $\text{cm}^{-1}$  are attributed to imidazole ring puckering, C5–N vibrations, methyl bending, and C4=C5 stretching, respectively, which are similar to the observation of Tanaka et al. [52]. The remaining spectra can be assigned to stretching and bending on the imidazole ring [27]. With doping of Zr into the ZIF-8 frameworks, the peaks at 1116 and 1484 disappeared with no significant change in main peaks on spectra [53]. The spectra of three samples shows similar vibration modes, which confirms structural equality in the frameworks.

379

380  
381

**Figure 10.** Raman spectra of the crystal-size ZIF-8 and Zr/ZIF-8 and recycled Zr/ZIF-8 samples.

382

383

384

385

386

387

388

389

390

391

392

393

394

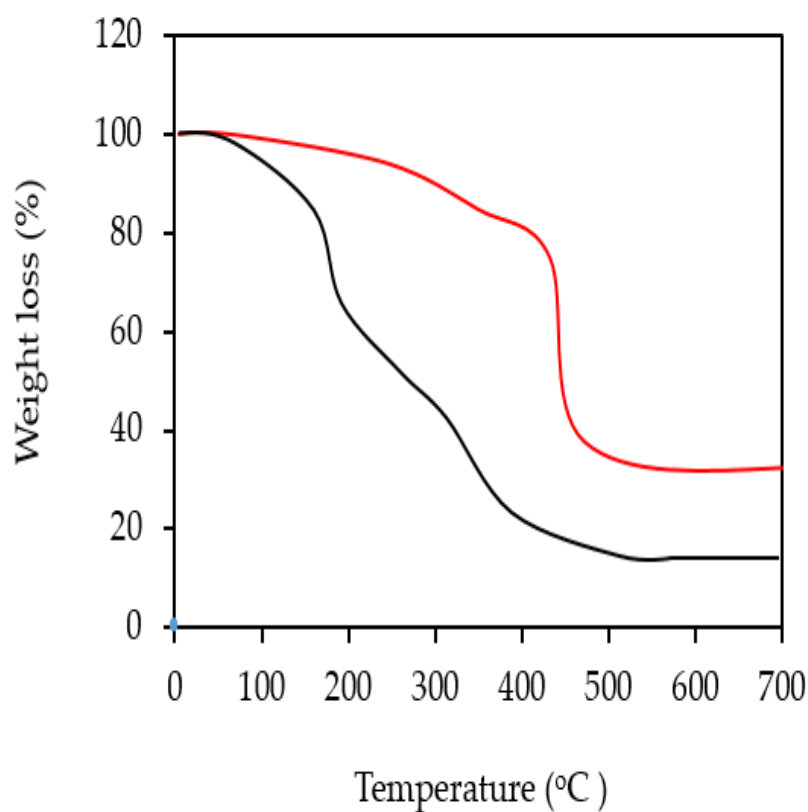
395

396

397

398

There are three distinct phases of weight loss experienced by both samples as indicated in Figure 11. It can be observed from the thermogram that both catalysts experienced a very small initial weight loss of about 3% in the region from 298 to 373 K in the first phase. This can be attributed to loss of water and some guest molecules (e.g. methanol) and possibly some unreacted species trapped in the pore cavities of the framework. As the temperature was further increased through the second phase, Zr/ZIF-8 experienced a gradual and steady weight loss up to 723 K and then remained stable thereafter until 973 K. Conversely, ZIF-8 experienced a rapid and significant weight loss of around 54% up to 823 K attributing the decomposition of some absorbed organic ligand and the final weight loss phase experienced the collapse of the ZIF-8 structure at high temperature [54]. It is worth noting that materials stability of ZIF-8 framework can be attributed to the incorporation of zirconium in ZIF-8. A similar observation was reported by Cavka et al. [44] in the doping of Lanthanum into ZIF-8. After the decomposition, approximately 39% of the starting weight remained. From this observation, it can be concluded that the Zr/ZIF-8 catalyst frameworks have remained structurally stable and this is consistent with the XRD and SEM.



399  
400 **Figure 11.** Thermal stability curve of ZIF-8 and Zr/ZIF-8.

401 **4. Catalytic activity**

402 After catalyst characterization, the catalytic activity of the novel materials was compared with ZIF-  
403 8 for the synthesis of chloromethyl ethylene carbonate from CO<sub>2</sub> and epichlorohydrin under solvent-  
404 free conditions. It is interesting to note that the combination of acid and basic sites (Lewis and  
405 Brönsted site) existing in the MOF catalyst may improve the catalytic activity of both samples. The  
406 reactions were carried out under the same conditions of 353 K reaction temperature, 8 bar CO<sub>2</sub>  
407 pressure, 10% (w/w) catalyst loading, 8 h reaction time and 350 rpm of stirring speed.  
408

409 **Table 2:** Summary of catalytic performance of ZIF-8 and Zr/ZIF-8 for coupling reaction of CO<sub>2</sub> and  
 410 epichlorohydrin to produce chloromethyl ethylene carbonate

Entr y	Catalyst	T (K)	Conversion (%)	Selectivity (%)	Yield (%)
1	ZIF-8	323	65	57	37
2	ZIF-8	333	69	64	44
3	ZIF-8	343	73	69	49
4	ZIF-8	353	77	77	52
5	ZIF-8	363	81	71	51
6	ZIF-8	373	85	69	49
7	Zr/ZIF-8	323	80	67	58
8	Zr/ZIF-8	333	86	74	64
9	Zr/ZIF-8	343	90	80	70
10	Zr/ZIF-8	353	93	86	76
11	Zr/ZIF-8	363	95	85	75
12	Zr/ZIF-8	373	97	82	72

411 From the Table 2, it follows that at optimum CO<sub>2</sub> pressure of 8 bar, reaction time of 8 h, catalyst  
 412 loading of 10 % w/w and variable temperature, Zr/ZIF-8 exhibits a higher catalytic activity than  
 413 ZIF-8 (Zr/ZIF-8: 93%, 86%, 76%; and ZIF-8: 77%, 77%, 52%) for conversion, selectivity and yield  
 414 respectively at the same reaction conditions. The presence of acid and/or basic site in heterogeneous  
 415 catalyst has significantly catalysed the reaction of CO<sub>2</sub> and ECH to produce CMEC [55].

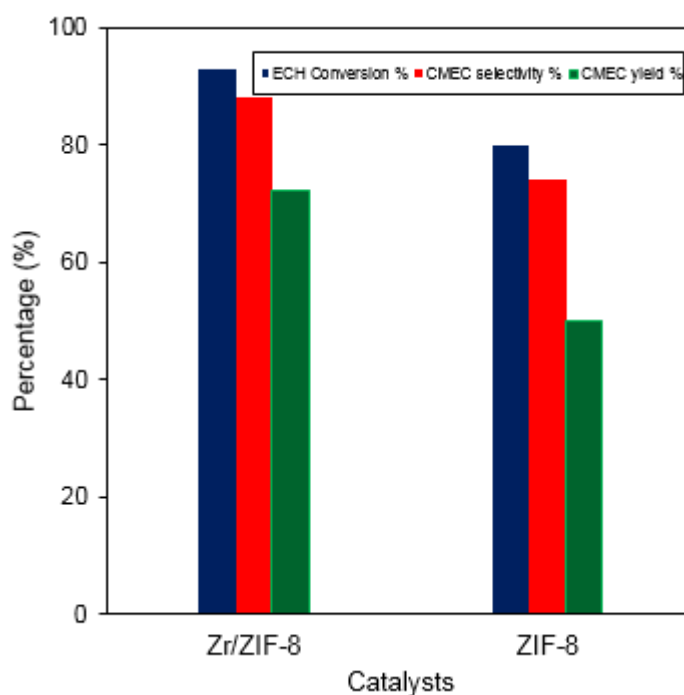
#### 416 4.1 Effect of different heterogeneous catalysts

417 Catalysts are very important parts of any chemical reaction; they contain active sites, which are  
 418 able to speed up the kinetics of chemical reaction by reducing the activation energy. Different types  
 419 of homogenous and heterogeneous catalysts have been synthesized to catalyse the reaction of CO<sub>2</sub>  
 420 and epoxide to produce corresponding organic carbonates. In order to assess the stability and  
 421 effectiveness of the samples, the catalytic activity of both ZIF-8 and Zr/ZIF-8 was investigated in the  
 422 synthesis of chloromethyl ethylene carbonate from CO<sub>2</sub> and epichlorohydrin. Table 2 shows the  
 423 effects of the two catalysts for the conversion of epichlorohydrin, selectivity and yield of  
 424 chloromethyl ethylene carbonate. The catalysts were synthesised using solvothermal method as per  
 425 standard procedures. The samples were heat-treated at about 373 K in order to enhance an improved  
 426 catalytic activity and were labelled as ZIF-8 and Zr/ZIF-8 for pure and doped samples respectively.  
 427 The reaction of CO<sub>2</sub> and ECH to produce CMEC was carried out in a 25 mL high-pressure reactor at  
 428 353 K reaction temperature, 8 bar CO<sub>2</sub> pressure, 10% catalyst loading and 8 h reaction time. It can be  
 429 seen from Table 2 that when ZIF-8 was used to catalyse the reaction of CO<sub>2</sub> and ECH, the conversion

430 of ECH, selectivity and the yield of CMEC were 88%, 82% and 56% respectively. However,  
 431 incorporating zirconium into ZIF-8 has significantly increased catalytic performance of Zr/ZIF-8 with  
 432 the conversion of ECH, selectivity and the yield of CMEC being 93%, 91% and 68% respectively,  
 433 although, the presence of side products were reported in both reactions by GC analysis. These side  
 434 products include 3-chloropropane 1,2-diol and 2,5-bis (chloromethyl)-1,4-dioxane.

435 With similar pore spaces and same embedded Lewis acid metal sites in both ZIF-8 and Zr/ZIF-8  
 436 catalysts, the increase in the catalytic activity of Zr/ZIF-8 may be ascribed to high CO<sub>2</sub> affinity *via* the  
 437 introduction of zirconium into MOF, which has significantly increased those pore spaces of ZIF-8  
 438 [56]. A fine balance of proximity between pure and Zr -doped MOF was critically examined by Demir  
 439 et al. (2017) [19]. Their experimental results in the solvent-free coupling reaction of ECH and CO<sub>2</sub> to  
 440 produce epichlorohydrin carbonate (ECHC) concluded that 79.6% yield of ECHC and 97.3%  
 441 selectivity were achieved after 2 h using Zr-MOF catalyst (Zr/MOF-53). It is however interesting to  
 442 note that GC analysis of the product of Zr/ZIF-8 identified 3-chloropropane-1,2-diol (diols of  
 443 epichlorohydrin- 14.2%) as the main reaction by-products.

444 To affirm the superior catalytic performance of Zr/ZIF-8 over ZIF-8, nitrogen adsorption and  
 445 desorption isotherms of the two frameworks were collected and presented in table 1. Zr/ZIF-8  
 446 showed higher CO<sub>2</sub> adsorption capacity which explains in part the improved catalytic performance.



447

448 **Figure 12.** Effect of different catalysts on the cycloaddition reaction of ECH and CO<sub>2</sub> to produce  
 449 CMEC with reaction conditions of 353 K reaction temperature, 8 bar CO<sub>2</sub> pressure, 10% catalyst  
 450 loading, 8 h reaction time and 350 rpm of stirring speed.

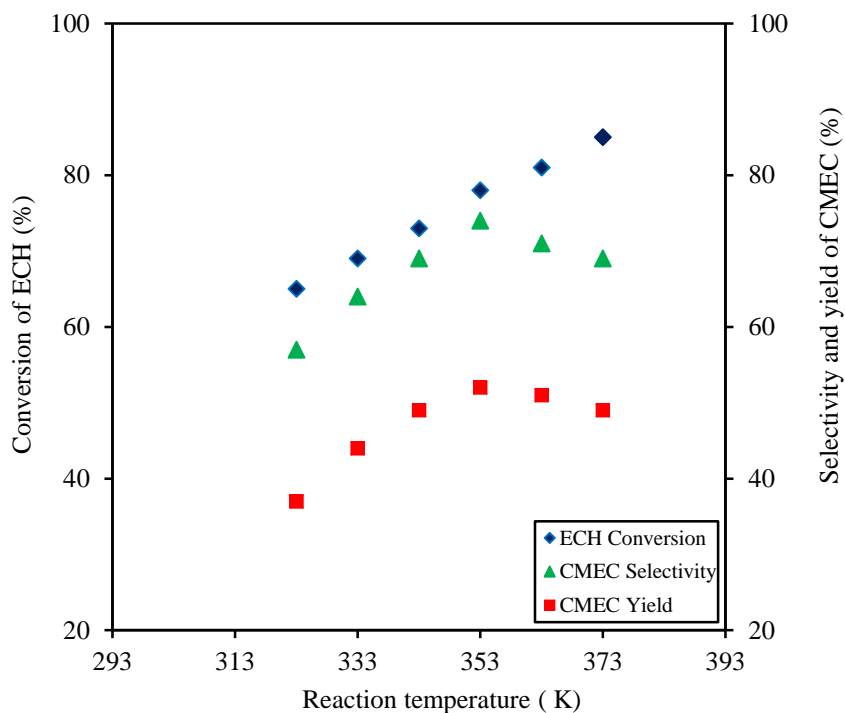
#### 451 4.2. Effect of temperature

452 The cycloaddition reaction of CO<sub>2</sub> and epoxide can be referred to as exothermic in nature. The  
 453 influence of temperature on the cycloaddition of CO<sub>2</sub> to ECH to produce CMEC was investigated  
 454 between temperature ranges of 323 to 373 K. All experiments were conducted with optimised reaction  
 455 conditions, which were determined during our previous studies with a 10% catalyst loading and 8  
 456 bar CO<sub>2</sub> pressure for 8 h and a stirring speed of 350 rpm. Table 2 shows the catalytic performance of  
 457 Zr/ZIF-8 and ZIF-8 as a function of temperature, CO<sub>2</sub> pressure, reaction time and catalyst loading. It  
 458 can be depicted from Figure 13 that the conversion of epichlorohydrin, selectivity and yield of CMEC  
 459 were temperature-dependent. Generally speaking, variation in temperature has similar trends in the  
 460 catalytic activity of both frameworks; the conversion of epichlorohydrin, the selectivity and yield of

461 CMEC increases as temperature increases from 323 to 353 K. However, incorporating zirconium into  
462 ZIF-8 has significantly improved the performance of Zr/ZIF-8 with the conversion of ECH, selectivity  
463 and yield of CMEC as 93%, 86% and 76% respectively, while ZIF-8 gave a conversion of ECH,  
464 selectivity and yield of CMEC as 77%, 74% and 52% respectively under the same optimum reaction  
465 temperature.

466 Further increase in reaction temperature beyond 353 K was unfavourable to selectivity and yield  
467 of CMEC in both systems. A slight decrease of the CMEC yield (from 76% to 75%; Zr/ZIF-8 and 52%  
468 to 51%; ZIF-8) was observed upon an increase in temperature. This may be due to the formation of  
469 diols and dimers of epichlorohydrin [57] and a small amount of by-products such as polymerized  
470 CMEC could also affect the yield. Adeleye et al. [5] reported that the increase in the reaction  
471 temperature caused a decrease in carbonate yield, due to the decomposition of the catalyst at a higher  
472 temperature. Kim et al. [58] also concluded that the reaction temperature for optimal performance is  
473 dependent on the nature of the catalyst employed. Therefore, for this set of experiments, the  
474 optimized reaction temperature for both frameworks in the synthesis of chloromethyl ethylene  
475 carbonate was 353 K. All the subsequent experiments for the chloromethyl ethylene carbonate were  
476 conducted at 353 K.

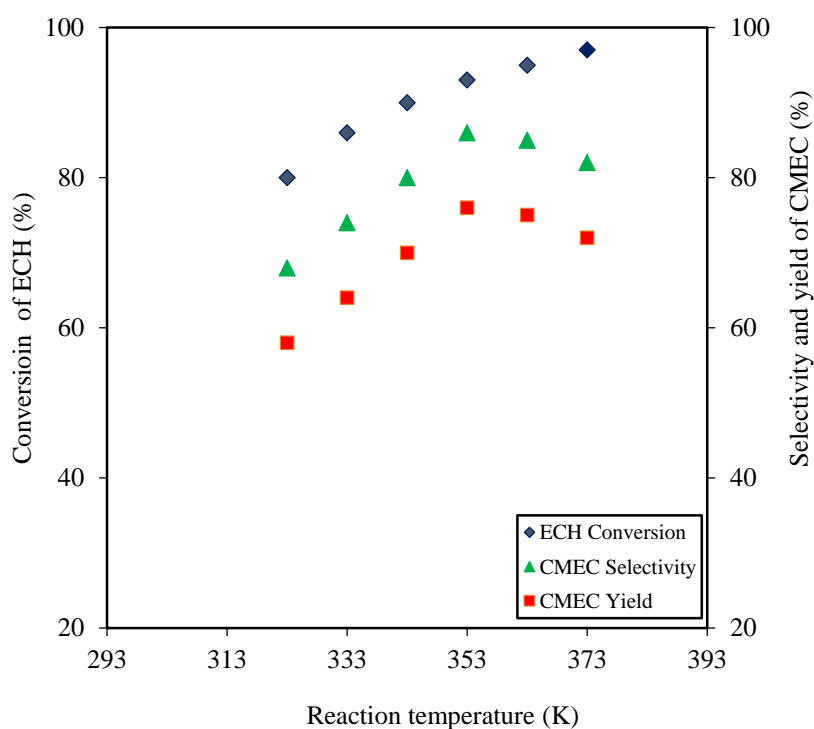
477  
478  
479  
480  
481  
482  
483  
484  
485  
486  
487  
488  
489  
490  
491  
492  
493  
494



495

496

(a) ZIF-8



497

498

(b) Zr/ZIF-8

499 **Figure 13.** Temperature dependence on conversion of epichlorohydrin (ECH) *versus* selectivity and  
 500 yield of chloromethyl ethylene carbonate (CMEC). Experimental conditions: catalyst (a) ZIF-8 and  
 501 (b) Zr/ZIF-8; catalyst loading 10% (w/w); reaction time 8 h; CO<sub>2</sub> pressure 8 bar; stirring speed 350  
 502 rpm.

503 4.3 Effect of CO<sub>2</sub> pressure

504 CO<sub>2</sub> pressure is another important factor influencing the cycloaddition of CO<sub>2</sub> to epoxides. The  
505 pressure of carbon dioxide has been established as one of the most crucial factors affecting the  
506 conversion, yield and selectivity of cyclic carbonate [59]. The reaction of epichlorohydrin and CO<sub>2</sub> to  
507 produce chloromethyl ethylene carbonate was examined by varying the CO<sub>2</sub> pressures. For this  
508 study, the experiments were carried out at 353 K, 10% catalyst loading and 350 rpm for 8 h.

509 The selectivity and yield of CMEC was found to increase steadily from 67% and 58% to 86% and  
510 76%, respectively as the CO<sub>2</sub> pressure increases from 2 to 8 bar. These results indicate that the catalytic  
511 performance of the Zr/ZIF-8 depends on the concentration of available CO<sub>2</sub> at the reactive sites.  
512 Similar variation was observed in the catalytic activity of the two frameworks with changing CO<sub>2</sub>  
513 pressure where the selectivity and yield of CMEC increased from 57% and 37% to 77% and 52%  
514 respectively at the same pressure of 8 bar of CO<sub>2</sub> as in the case of Zr/ZIF-8.

515 Figure 14 demonstrates the dependence of CO<sub>2</sub> pressure on the yield of CMEC. It can be  
516 observed from the graph that the CMEC yield increased with increasing pressure, the maximum of  
517 the CMEC yield was reached at 8 bar. By increasing the CO<sub>2</sub> pressure more than 8 bar, a negative  
518 effect was observed on both reaction systems, where both yield and conversion experience a slight  
519 drop. Wang et al. [60] observed that the introduction of too much CO<sub>2</sub> dissolves in epoxide may result  
520 in the formation of CO<sub>2</sub>-epoxide complex, and retards the interaction resulting in a lower conversion.  
521 Similar results were also reported by Onyenkeadi et al. [61]; Adeleye et al. [62] where the introduction  
522 of higher pressure of CO<sub>2</sub> dissolved in the epoxide and becomes an unfavourable factor due to the  
523 difficulty of separating CO<sub>2</sub> and ECH. This condition inhibits the reaction between ECH and catalyst,  
524 thus resulting in lower yield [63]. Zanon et al. [43] also reported that many diols and dimers of  
525 epichlorohydrin were produced as side products at high pressure. Based on the experimental results  
526 and theoretical study, it can be concluded that 8 bar CO<sub>2</sub> pressure was the optimum and all  
527 subsequent experiments for the CMEC synthesis were carried out at a CO<sub>2</sub> pressure of 8 bar.

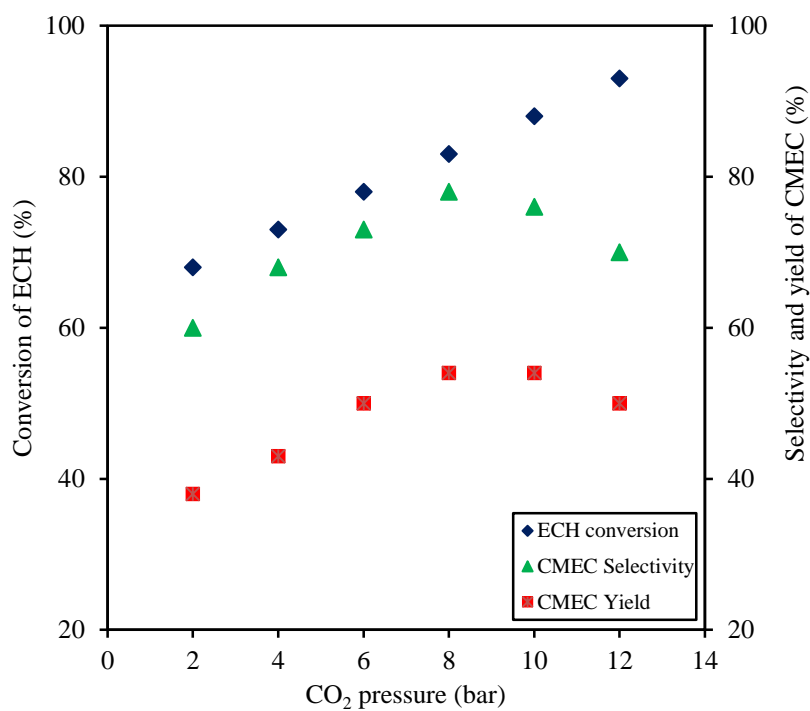
528

529

530

531

532

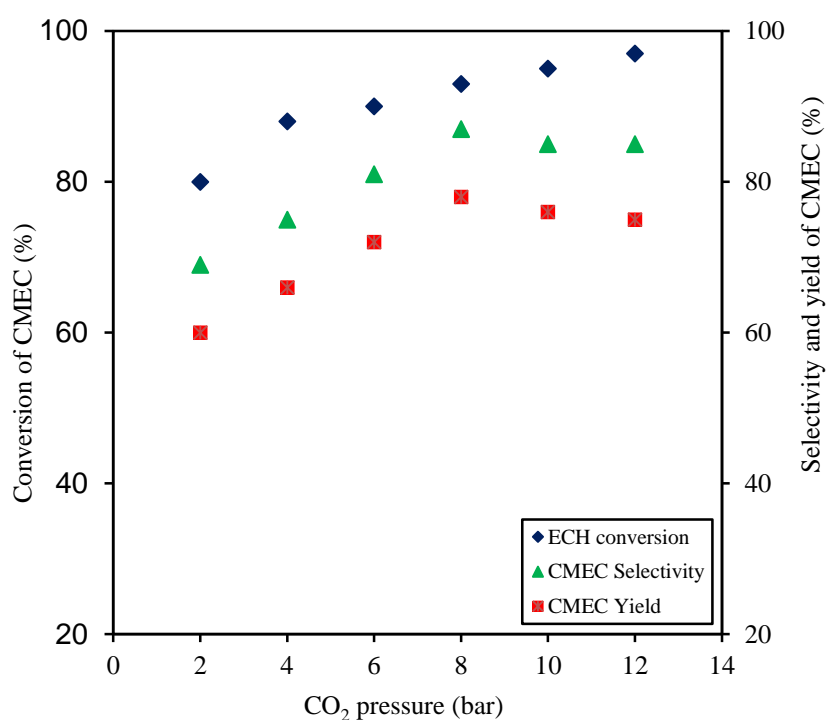


533

534

(a) ZIF-8

535



536

537

(b) Zr/ZIF-8

538

539

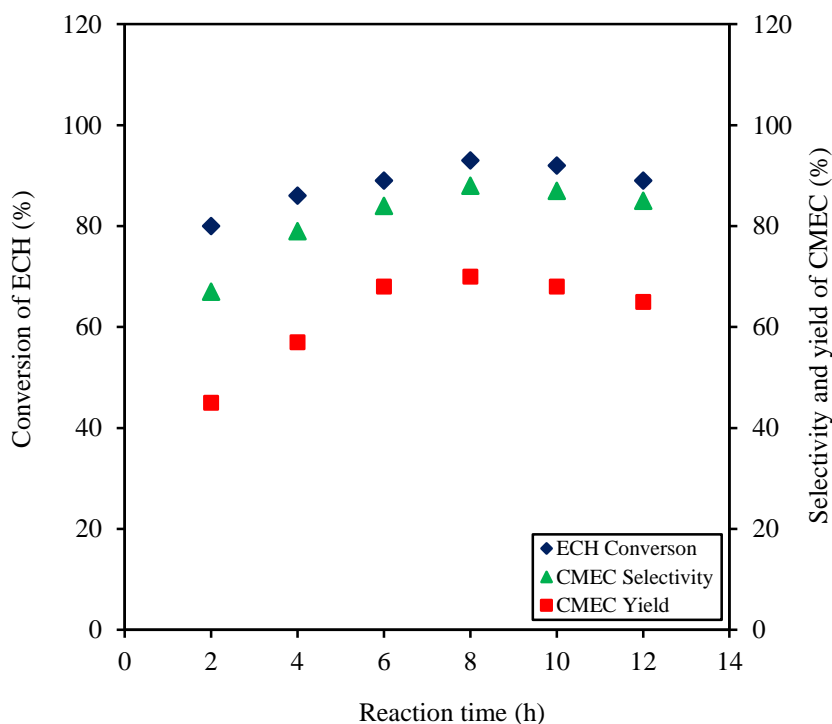
540

541

**Figure 14.** Pressure dependence on conversion of epichlorohydrin (ECH) *versus* selectivity and yield of chloromethyl ethylene carbonate (CMEC). Experimental conditions: catalyst (a) ZIF-8 and (b) Zr/ZIF-8; catalyst loading 10% (w/w); reaction time 8 h; reaction temperature 353 K; stirring speed 350 rpm.

## 542 4.4. Influence of reaction time

543 The effect of varying the reaction time on the yield of CMEC was investigated by carrying out a set  
 544 of coupling reaction of CO<sub>2</sub> and epichlorohydrin using both ZIF-8 and Zr/ZIF-8 catalysts. For this  
 545 study, all experiments were conducted at 353 K and 8 bar CO<sub>2</sub> pressure with 10% (w/w) catalyst  
 546 loading of ZIF-8 and Zr/ZIF-8. Figure 15 demonstrates the influence of reaction time on CMEC yield  
 547 and selectivity. The results shown on the graph illustrates that the yield increased continuously at  
 548 the beginning and reached 76% and 52% within 8 h for Zr/ZIF-8 and ZIF-8, then decreased to 75%  
 549 and 51% respectively indicating that a slight change in the reaction condition can influence the  
 550 product formation in a reaction. Similarly, the conversion of ECH was observed to increase from  
 551 353 K to 366 K when the reaction time was increased from 2 h to 8 h. However, when the reaction  
 552 time was increased further to 10 h and above, a progressive decrease in conversion of ECH was  
 553 recorded. Similar observation has been previously reported in the conversion of ECH to  
 554 chloropropene carbonate with Zn-ZIF-67 by Zanon et al. [74]. According to him, conversion of  
 555 epoxides reaches an equilibrium plateau at optimum reaction time. This phenomenon is referred to  
 556 as induction period. Induction period is attained when the CO<sub>2</sub> and epoxides sufficiently diffuses  
 557 into the catalytic frameworks of ZIF-material to reach the active sites of the catalyst and then be  
 558 converted to the organic carbonate. Beyond the induction period, low conversion of epoxides as  
 559 well organic carbonates may be observed. From Figure 15, it can be concluded that prolonged  
 560 reaction time produces lesser ECH conversion and consequently lesser CMEC yield and selectivity.  
 561 Based on the experimental results and theoretical study, the reaction time of 8 h was considered the  
 562 optimum for ZIF-8 and Zr/ZIF-8.



563

564 **Figure 15.** Time dependence on conversion of epichlorohydrin (ECH) *versus* selectivity and yield of  
 565 chloromethyl ethylene carbonate (CMEC). Experimental conditions: catalyst Zr/ZIF-8; catalyst  
 566 loading 10% (w/w); reaction temperature 353 K; CO<sub>2</sub> pressure 8 bar; stirring speed 350 rpm.

#### 567 4.5. Effect of external mass transfer in heterogeneous catalytic processes

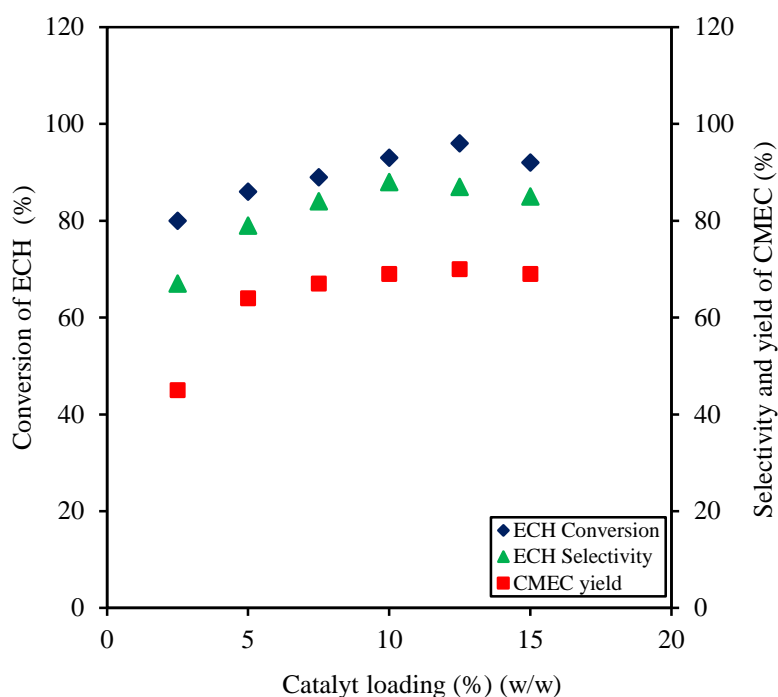
568 Mass transfer limitations play significant roles in chemical reactions by controlling the rate of  
569 reaction towards the desired product. In homogenous catalytic reaction, the effect of mass transfer  
570 between the phases is mostly negligible. However, in a heterogeneous catalytic reaction, the reaction  
571 rate significantly relies on the mass or diffusion between these phases. Mass transfer is typically  
572 higher in porous solid or fine particles of nanoscale than large nonporous catalyst [5,64], transfer of  
573 material from the exterior to the interior of a particle happens through pores that open to the  
574 external surface, which provides access to the interior of the crystallite material [19]. A typical  
575 example is zeolitic imidazolate framework (ZIF-8).

576 In the heterogeneous catalytic conversion of CO<sub>2</sub> and epoxide, the internal and external gradient  
577 of transport materials between system phases lowers the activity and selectivity of the catalyst  
578 towards the desired product [65]. It is important to know that when designing a new catalyst and  
579 directing such a catalyst to be selective towards a particular desired product mass transfer resistance  
580 and the kinetics are key functions [5]. In cycloaddition reaction of CO<sub>2</sub> with ECH, the physicochemical  
581 properties of the catalyst and the operating conditions all have a direct effect on the activity of the  
582 catalyst as well as the quality of CMEC formed [65]. When a chemical reaction occurs on an active  
583 surface, intraparticle diffusion takes place through the pores and the film surrounding the solid  
584 catalyst [66].

585 The coupling reaction of ECH with CO<sub>2</sub> to produce chloromethyl ethylene carbonate is an  
586 exothermic reaction. In order to reduce or eliminate the effects of mass transfer resistance, it is  
587 recommended to employ a highly porous heterogeneous catalyst [5]. The influence of mass transfer  
588 on the reaction of ECH and CO<sub>2</sub> to synthesise CMEC at 353 K reaction temperature for 8 h with a  
589 range of stirring speed between 320 and 550 rpm in an autoclave reactor. It was observed that there  
590 was no significant change in the conversion of ECH (~93), selectivity (~86) and the yield of CMEC  
591 (~76) when the stirrer speed was maintained above 330 rpm. Therefore, it was concluded that there  
592 was no effect of external mass transfer resistance on the experimental conditions.

#### 593 4.6 Effect of catalyst loading

594 To investigate the influence of catalyst loading on the CMEC synthesis, several number of  
595 experiments were performed by varying the molar ratio of both ZIF-8 and Zr/ZIF-8 catalyst to ECH.  
596 For this study, all experiments were conducted at 353 K and 8 bar CO<sub>2</sub> pressure for 8 h. The results  
597 of varying catalyst loading are presented in Figure 16. It can be observed from the graph that by  
598 increasing the catalyst loading, there was a corresponding increase in ECH conversion, yield and  
599 selectivity of CMEC. For example, for the experiments conducted with catalyst loadings from 2.5-  
600 7.5%, there was a significant increase in ECH conversion, yield and selectivity of CMEC. Also, for  
601 the experiment conducted at 10% (w/w) of catalyst loading, there was a sharp increase of ECH  
602 conversion, yield and selectivity of CMEC from 90-96%, 45-56% and 73-79%, respectively.  
603 According to Adeleye et al. [65], the decrease in epoxide conversion may be ascribed to a decrease  
604 in the substrate concentration around the pore cavities of the catalyst at higher catalyst loading. This  
605 effect neutralizes the Brønsted acid centers of the catalyst thereby preventing the interaction  
606 between the acidic sites of the catalyst and the oxygen atom of epoxide from the ring opening. This  
607 consequently reduces the epoxides conversion to organic carbonates. Considering the percentage  
608 error of ±2% it can be concluded that the number of active sites for ECH and CO<sub>2</sub> to react and  
609 produce CMEC was large enough at 10% (w/w) catalyst loading. From the results obtained with  
610 respect to catalyst loading, 10% (w/w) was the optimum. From the experimental results for both  
611 ZIF-8 and Zr/ZIF-8 catalysts, it is satisfactory to conclude that 10% (w/w) catalyst loading was  
612 considered the optimum and further experiments were carried out at 10% (w/w) catalyst loading.



613

614 **Figure 16.** Catalyst loading dependence on conversion of epichlorohydrin (ECH) *versus* selectivity  
 615 and yield of chloromethyl ethylene carbonate (CMEC). Experimental conditions: catalyst Zr/ZIF-8;  
 616 reaction temperature 353 K, (w/w); reaction time 8 h; CO<sub>2</sub> pressure 8 bar; stirring speed 350 rpm.

#### 617 4.7. Effect of reaction conditions on catalysts selectivity to chloromethyl ethylene carbonate

618 Figures 13 (a) and (b) shows the effect of varying reaction temperature on catalysts' selectivities  
 619 towards CMEC. For example, it can be observed that when the temperature was increased from 50  
 620 °C to 80 °C, both catalysts show a corresponding increase in selectivities from 68% and 50% to 86%  
 621 and 74%, respectively. However, when the temperature was increased beyond the 353 K, a marginal  
 622 decrease in selectivities were observed in both frameworks, demonstrating that the 353 K was the  
 623 optimum temperature for the reaction. Meanwhile, the gas chromatography-mass spectroscopy (GC-  
 624 MS) analysis of the samples shows that 17.3% of 2,5-bis (chloromethyl)-1,4-dioxane (by-product) has  
 625 been formed at 353 K, this may explain in part why a drop in catalysts' selectivities was recorded for  
 626 both samples. Similar results and by-product have been previously reported with ZIF-8 by Mousavi  
 627 et al. [67]. Miralda et al. [68], also agrees that almost 100% selectivity of ZIF-8 to chloropropene  
 628 carbonate was achieved at a temperature of 393 K, but decreased to 78.6% when the temperature was  
 629 increased to 403 K.

630 In addition to the effect of temperature on catalysts' selectivities, the influence of varying CO<sub>2</sub>  
 631 pressure on catalysts' selectivities was also investigated. According Figures 14 (a) and (b), the  
 632 selectivity of the catalysts towards CMEC was found to increase steadily from 67% and 58% to 86%  
 633 and 76%, respectively as the CO<sub>2</sub> pressure was increased from 2 to 8 bar. These results indicates that  
 634 the activity and selectivity of both catalysts were influenced by the concentration of available CO<sub>2</sub>  
 635 at the reactive sites. Although, similar effect was observed in the responses of both catalysts to variation  
 636 in CO<sub>2</sub> pressure, however, the results shows that Zr/ZIF-8 has higher selectivity than ZIF-8 catalyst,

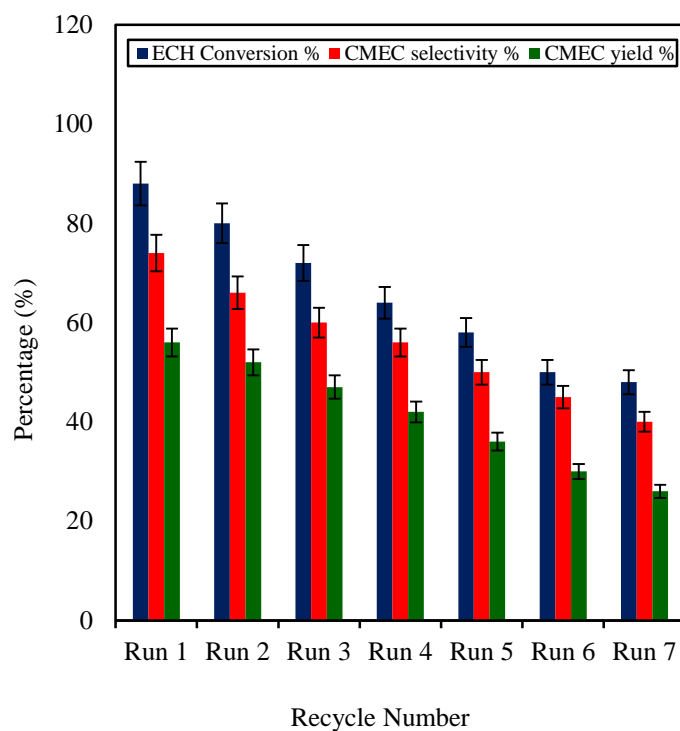
637 where the selectivity of both catalysts increased from 69% and 60% to 87% and 77%, respectively for  
638 Zr/ZIF-8 and ZIF-8 catalysts. Conversely, both samples experienced decline in selectivities from 87%  
639 and 77% to 85% and 70% for ZIF-8 and Zr/ZIF-8 respectively when the CO<sub>2</sub> pressure was increased  
640 beyond the optimum level of 8 Bar.

641 Miralda et al. [68], further argues that ZIF-8 is a dual-functional catalyst with both acidic and  
642 basic sites that have been associated with the Lewis acid Zn<sup>2+</sup> ions and the basic imidazole groups,  
643 respectively. This bifunctional characteristic enhances the catalyst selectivity for cycloaddition  
644 reaction. In a separate report, Carreon et al. [69], also ascertained that it is likely that Lewis acid sites  
645 associated with Zn<sup>2+</sup> ions in the ZIF-8 framework play the vital role in catalysing the reaction of  
646 epichlorohydrin and CO<sub>2</sub> to chloropropene carbonate. They further explained that the presence of  
647 basic nitrogen atoms of the imidazole ligand, probably, favours the adsorption and binding of CO<sub>2</sub>  
648 as well as activation of the carbon-oxygen bonds in CO<sub>2</sub>. In agreement with other similar doped ZIF-  
649 8, the open metal centers in the Zr/ZIF-8 has the potential to easily activate the epoxides and the basic  
650 sites present in the frameworks. This could be the reason for the higher selectivity that were observed  
651 in the solvent-free ECH-CO<sub>2</sub> cycloaddition reactions under mild conditions [70]. Comparatively, the  
652 higher selectivity of Zr/ZIF-8 than ZIF-8 towards CMEC may be attributed to the presence of  
653 zirconium (Zr). According to a 2019 publication by de Caro et al. [71], the effect of Zr doping on Mg-  
654 Al hydrotalcite the catalyst has significantly increased its selectivity from 90% to >99% towards  
655 glycerol carbonate (GC).

#### 656 4.8. Reusability of ZIF-8 catalysts

657 Reusability is an important and essential feature of any heterogeneous catalyst in order to be  
658 considered useful in industrial applications [52]. The influence of catalyst reusability on the catalytic  
659 properties of ZIF-8 and Zr/ZIF-8 in the cycloaddition reaction was investigated. The experiments  
660 were carried out in a high-pressure reactor at optimum reaction conditions, i.e. at 353 K, 8 bar with  
661 fresh 10% (w/w) ZIF-8 catalyst loading, for 8 h and at a stirring speed of 350 rpm. The catalysts after  
662 Run 1 in the cycloaddition reaction were washed with ethanol and acetone, centrifuged, and oven-  
663 dried at 343 K for 12 h before reuse. The recovered catalysts were reused for up to 7 subsequent  
664 experiments following the same experimental procedure. ZIF-8 showed a progressive loss in  
665 catalytic activity after each runs as shown in Figure 17 while Zr/ZIF-8 exhibited no loss of activity  
666 indicating the catalyst stability for cycloaddition reaction of CO<sub>2</sub> epichlorohydrin. Yuan et al. [72]  
667 stated that the presence of dopant in ZIF-8 show that zirconium is more stable and resilient during  
668 the reaction. There was no significant change in the conversion of ECH, selectivity and yield of  
669 CMEC using Zr/ZIF-8. Although, a very slight decrease in the yield of CMEC from 70% (fresh) to  
670 69% (recycled) was observed. The low catalytic activity of the recycled Zr/ZIF-8 catalyst may be  
671 ascribed to formation of carbonaceous materials during the cycloaddition reaction as previously  
672 reported by Bosch et al. [73]. Furthermore, the XRD and FT-IR analyses results confirmed that  
673 Zr/ZIF-8 maintained its crystallinity throughout the reaction process.

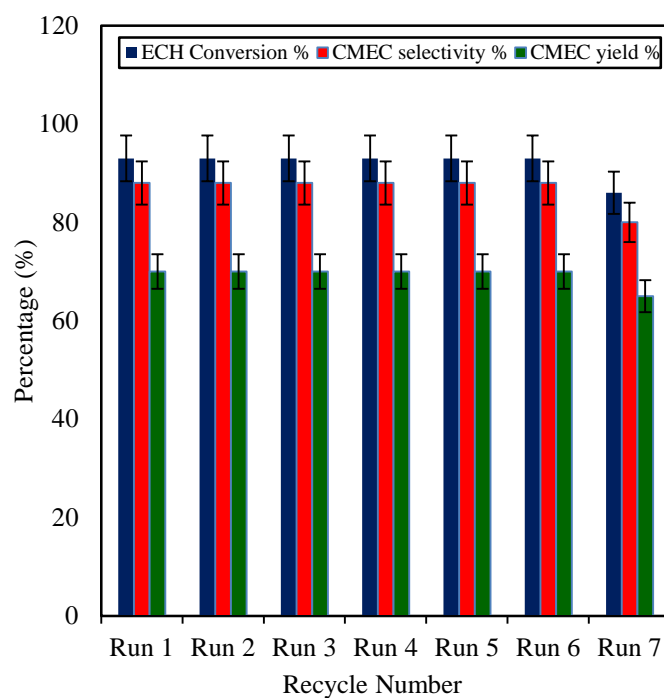
674  
675  
676  
677



678

679

(a) ZIF-8



680

681

(b) Zr/ZIF-8

682 **Figure 17.** Catalyst reusability studies on conversion of epichlorohydrin (ECH), selectivity and yield  
 683 of chloromethyl ethylene carbonate (CMEC). Experimental conditions: catalyst: (a) ZIF-8 and (b)  
 684 Zr/ZIF-8; catalyst loading 10% (w/w); temperature 353 K; CO<sub>2</sub> pressure 8 bar; reaction time 8 h;  
 685 stirring speed 350 rpm.

686

## 687 5. Conclusions

688 Zr/ZIF-8 has been successfully designed and assessed as a greener and highly efficient CO<sub>2</sub>-  
689 reduction catalyst for the synthesis of CMEC. Although ZIF-8 is criticized by many researchers as  
690 thermally unstable for the synthesis of organic carbonates from CO<sub>2</sub> and epoxide, however, our  
691 experiments have confirmed that the introduction of zirconium into ZIF-8 could strengthen the weak  
692 functionality, making it tenable for large-scale industrial applications. Several authors have utilized  
693 zirconium to reinforce different kinds of MOF experiments in order to achieve optimum results.  
694 However, their attempts have been unsatisfactory, partly because a firm balance between the  
695 required percentage of zirconium dopant and their host molecules were not established for those  
696 particular experiments. It may also be worth mentioning that this work has utilized a 10% dopant of  
697 zirconium for such a tremendous catalytic activity of Zr/ZIF-8. The stability tests carried out on both  
698 samples show that Zr/ZIF-8 demonstrates higher stability compared with single metal ZIF-8.

699 It has been concluded from the experimental results that there is a direct relationship between  
700 variation in the reaction conditions and ECH conversion, CMEC yield and selectivity. From the  
701 experimental results, it can be observed that Zr/ZIF-8 catalyst displayed high epoxide conversions  
702 and high selectivity to chloromethyl ethylene carbonate at 353 K, without using any solvent or co-  
703 catalyst. Lewis acid copper (II) sites in the ZIF-8 frameworks promote adsorption of CO<sub>2</sub> on the solid  
704 surface and its further conversion to CMEC. The activity of reused Zr/ZIF-8 catalyst showed  
705 consistent stability over seven subsequent runs. The optimum reaction condition for the experiments  
706 was found at 353 K, 8 bar CO<sub>2</sub> pressure and 8 h using fresh 10% (w/w) Zr/ZIF-8 catalyst loading for  
707 this reaction. Therefore, the development of a novel Zr/ZIF-8 catalyst for the synthesis of CMEC from  
708 CO<sub>2</sub> and ECH provided an efficient and promising greener route for CO<sub>2</sub> utilisation.

## 709 6. Acknowledgements

710 Bisi Olaniyan is immensely grateful to the School of Engineering, LSBU, UK for partial financial  
711 assistance rendered throughout this research work.

712  
713  
714  
715  
716  
717  
718  
719  
720  
721  
722  
723  
724  
725  
726  
727  
728  
729  
730  
731  
732

733 **References**

- 734 1. Dai, W.L.; Luo, S.L.; Yin, S.F.; Au, C.T. The direct transformation of carbon dioxide to  
735 organic carbonates over heterogeneous catalysts. *Appl. Catal. A Gen.* **2009**, *366*, 2–12.
- 736 2. Saada, R.; AboElazayem, O.; Kellici, S.; Heil, T.; Morgan, D.; Lampronti, G.I.; Saha, B.  
737 Greener synthesis of dimethyl carbonate using a novel tin-zirconia/graphene nanocomposite  
738 catalyst. *Appl. Catal. B Environ.* **2018**, *226*, 451–462.
- 739 3. Baj, S.; Krawczyk, T.; Jasiak, K.; Siewniak, A.; Pawlyta, M. Catalytic coupling of epoxides  
740 and CO<sub>2</sub> to cyclic carbonates by carbon nanotube-supported quaternary ammonium salts.  
741 *Appl. Catal. A Gen.* **2014**, *488*, 96–102.
- 742 4. Gong, Q.; Luo, H.; Cao, D.; Zhang, H.; Wang, W.; Zhou, X. Efficient cycloaddition reaction of  
743 carbon dioxide with epoxide by Rhodamine based catalyst under 1 atm pressure. *Bull.*  
744 *Korean Chem. Soc.* **2012**, *33*, 1945–1948.
- 745 5. Adeleye, A.I.; Kellici, S.; Heil, T.; Morgan, D.; Vickers, M.; Saha, B. Greener synthesis of  
746 propylene carbonate using graphene-inorganic nanocomposite catalysts. *Catal. Today* **2015**,  
747 *256*, 347–357.
- 748 6. Onyenkeadi, V.; Kellici, S.; Saha, B. Greener synthesis of 1,2-butylene carbonate from CO<sub>2</sub>  
749 using graphene-inorganic nanocomposite catalyst. *Energy* **2018**, *165*, 867–876.
- 750 7. Kathalikkattil, A.C.; Babu, R.; Tharun, J.; Roshan, R.; Park, D.W. Advancements in the  
751 Conversion of Carbon Dioxide to Cyclic Carbonates Using Metal Organic Frameworks as  
752 Catalysts. *Catal. Surv. from Asia* **2015**, *19*, 223–235.
- 753 8. Karagiari, O.; Lalonde, M.B.; Bury, W.; Sarjeant, A.A.; Farha, O.K.; Hupp, J.T. Opening  
754 ZIF-8: A catalytically active zeolitic imidazolate framework of sodalite topology with  
755 unsubstituted linkers. *J. Am. Chem. Soc.* **2012**, *134*, 18790–18796.
- 756 9. Beyzavi, M.H.; Stephenson, C.J.; Liu, Y.; Karagiari, O.; Hupp, J.T.; Farha, O.K. Metal  
757 Organic Framework-Based Catalysts: Chemical Fixation of CO<sub>2</sub> with Epoxides Leading to  
758 Cyclic Organic Carbonates. *Front. Energy Res.* **2015**, *2*, 1–10.
- 759 10. Rimoldi, M.; Howarth, A.J.; Destefano, M.R.; Lin, L.; Goswami, S.; Li, P.; Hupp, J.T.; Farha,  
760 O.K. Catalytic Zirconium/Hafnium-Based Metal-Organic Frameworks. *ACS Catal.* **2017**, *7*,  
761 997–1014.
- 762 11. Zhang, X.; Zhang, X.; Johnson, J.A.; Chen, Y.S.; Zhang, J. Highly Porous Zirconium Metal-  
763 Organic Frameworks with β-UH<sub>3</sub>-like Topology Based on Elongated Tetrahedral Linkers. *J.*  
764 *Am. Chem. Soc.* **2016**, *138*, 8380–8383.
- 765 12. Jeong, H.-M.; Roshan, R.; Babu, R.; Kim, H.-J.; Park, D.-W. Zirconium-based isorecticular  
766 metal-organic frameworks for CO<sub>2</sub> fixation via cyclic carbonate synthesis. *Korean J. Chem.*  
767 *Eng.* **2017**, *35*, 438–444.

- 768 13. Yang, X.; Qiu, L.; Luo, X. ZIF-8 derived Ag-doped ZnO photocatalyst with enhanced  
769 photocatalytic activity. *RSC Adv.* **2018**, *8*, 4890–4894.
- 770 14. Bai, Y.; Dou, Y.; Xie, L.-H.; Rutledge, W.; Li, J.-R.; Zhou, H.-C. Zr-based metal–organic  
771 frameworks: design, synthesis, structure, and applications. *Chem. Soc. Rev.* **2016**, *45*, 2327–  
772 2367.
- 773 15. Cavka, J.H.H.; Jakobsen, S.; Olsbye, U.; Guillou, N.; Lamberti, C.; Bordiga, S.; Lillerud, K.P.P.  
774 A New Zirconium Inorganic Building Brick Forming Metal Organic Frameworks with  
775 Exceptional Stability. **2008**, *130*, 13850–13851.
- 776 16. Marshall, R.J.; Forgan, R.S. Postsynthetic Modification of Zirconium Metal-Organic  
777 Frameworks. *Eur. J. Inorg. Chem.* **2016**, *2016*, 4310–4331.
- 778 17. Jin, Z.; Yang, H. Exploration of Zr–Metal–Organic Framework as Efficient Photocatalyst for  
779 Hydrogen Production. *Nanoscale Res. Lett.* **2017**, *12*, 850–854.
- 780 18. Cavka, J.H.H.; Jakobsen, S.; Olsbye, U.; Guillou, N.; Lamberti, C.; Bordiga, S.; Lillerud, K.P.P.  
781 A New Zirconium Inorganic Building Brick Forming Metal Organic Frameworks with  
782 Exceptional Stability. **2008**, *130*, 13850–13851.
- 783 19. Demir, S.; Usta, S.; Tamar, H.; Ulusoy, M. Solvent free utilization and selective coupling of  
784 epichlorohydrin with carbon dioxide over zirconium metal-organic frameworks. *Microporous*  
785 *Mesoporous Mater.* **2017**, *244*, 251–257.
- 786 20. Schejn, A.; Aboulaich, A.; Balan, L.; Falk, V.; Lalevée, J.; Medjahdi, G.; Aranda, L.; Mozet, K.;  
787 Schneider, R. Cu<sup>2+</sup> -doped zeolitic imidazolate frameworks (ZIF-8): efficient and stable  
788 catalysts for cycloadditions and condensation reactions. *Catal. Sci. Technol.* **2015**, *5*, 1829–  
789 1839.
- 790 21. Thi Thanh, M.; Vinh Thien, T.; Thi Thanh Chau, V.; Dinh Du, P.; Phi Hung, N.; Quang  
791 Khieu, D. Synthesis of Iron Doped Zeolite Imidazolate Framework-8 and Its Remazol Deep  
792 Black RGB Dye Adsorption Ability. *J. Chem.* **2017**, *2017*.
- 793 22. Coşkun, S.; Taşçı, Z.; Ulusoy, M.; Yurdakoç, M. Catalytic conversion of carbon dioxide into  
794 cyclic carbonates by Cu(II) and Ni(II) acetylacetonates anchored onto Siral 80. *Turkish J.*  
795 *Chem.* **2014**, *38*, 600–610.
- 796 23. Saada, R. (Supervisor-Saha. B) Catalytic conversion of carbon dioxide (CO<sub>2</sub>) into value  
797 added chemicals. PhD Thesis, *London South Bank University, London UK.* **2015**.
- 798 24. Gallardo-Fuentes, S.; Contreras, R.; Isaacs, M.; Honores, J.; Quezada, D.; Landaeta, E.;  
799 Ormazábal-Toledo, R. On the mechanism of CO<sub>2</sub> electro-cycloaddition to propylene oxides.  
800 *J. CO<sub>2</sub> Util.* **2016**, *16*, 114–120.
- 801 25. Nabipour, H.; Sadr, M.H.; Bardajee, G.R. Synthesis and characterization of nanoscale zeolitic  
802 imidazolate frameworks with ciprofloxacin and their applications as antimicrobial agents.

- 803 *New J. Chem.* **2017**, *41*, 7364–7370.
- 804 26. Fan, G.; Zheng, X.; Luo, J.; Peng, H.; Lin, H.; Bao, M.; Hong, L.; Zhou, J. Rapid synthesis of  
805 Ag/AgCl@ZIF-8 as a highly efficient photocatalyst for degradation of acetaminophen under  
806 visible light. *Chem. Eng. J.* **2018**, *351*, 782–790.
- 807 27. Li, Q.; Yang, W.; Li, F.; Cui, A.; Hong, J. Preparation of CoB/ZIF-8 supported catalyst by  
808 single step reduction and its activity in hydrogen production. *Int. J. Hydrogen Energy* **2018**,  
809 *43*, 271–282.
- 810 28. Nordin, N.A.H.M.; Ismail, A.F.; Mustafa, A. Synthesis and preparation of asymmetric  
811 PSf/ZIF-8 mixed matrix membrane for CO<sub>2</sub>/CH<sub>4</sub> separation. *J. Teknol. (Sciences Eng.* **2014**, *69*,  
812 *73–76*.
- 813 29. Zhu, M.; Srinivas, D.; Bhogeswararao, S.; Ratnasamy, P.; Carreon, M.A. Catalytic activity of  
814 ZIF-8 in the synthesis of styrene carbonate from CO<sub>2</sub> and styrene oxide. *Catal. Commun.* **2013**,  
815 *32*, 36–40.
- 816 30. Yao, J.; He, M.; Wang, K.; Chen, R.; Zhong, Z.; Wang, H. High-yield synthesis of zeolitic  
817 imidazolate frameworks from stoichiometric metal and ligand precursor aqueous solutions  
818 at room temperature. *CrystEngComm* **2013**, *15*, 3601–3606.
- 819 31. Schejn, A.; Aboulaich, A.; Balan, L.; Falk, V.; Lalevée, J.; Medjahdi, G.; Aranda, L.; Mozet, K.;  
820 Schneider, R. Cu<sup>2+</sup>-doped zeolitic imidazolate frameworks (ZIF-8): Efficient and stable  
821 catalysts for cycloadditions and condensation reactions. *Catal. Sci. Technol.* **2015**, *5*, 1829–  
822 1839.
- 823 32. Da Silva, J.D.S.F.; Malo, D.L.; Bataglion, G.A.; Eberlin, M.N.; Ronconi, C.M.; Alves, S.; De Sá,  
824 G.F. Adsorption in a fixed-bed column and stability of the antibiotic oxytetracycline  
825 supported on Zn(II)-[2-methylimidazolate] frameworks in aqueous media. *PLoS One* **2015**,  
826 *10*, 1371–1381.
- 827 33. Fang, Q.-R.; Makal, T.A.; Young, M.D.; Zhou, H.-C. Recent Advances in the Study of  
828 Mesoporous Metal-Organic Frameworks. *Comments Inorg. Chem.* **2010**, *31*, 165–195.
- 829 34. Cychosz, K.A.; Guillet-Nicolas, R.; García-Martínez, J.; Thommes, M. Recent advances in the  
830 textural characterization of hierarchically structured nanoporous materials. *Chem. Soc. Rev.*  
831 **2017**, *46*, 389–414.
- 832 35. Panchariya, D.K.; Rai, R.K.; Anil Kumar, E.; Singh, S.K. Core-Shell Zeolitic Imidazolate  
833 Frameworks for Enhanced Hydrogen Storage. *ACS Omega* **2018**, *3*, 167–175.
- 834 36. Liu, J.; He, J.; Wang, L.; Li, R.; Chen, P.; Rao, X.; Deng, L.; Rong, L.; Lei, J. NiO-PTA  
835 supported on ZIF-8 as a highly effective catalyst for hydrocracking of Jatropa oil. *Sci. Rep.*  
836 **2016**, *6*, 1–11.
- 837 37. Li-yan, N. a; Rui-nian, H.U. a; Gui-ling, N.; Xiao-xia, O.U. Nano / Micro HKUST-1

- 838 Fabricated by Coordination Modulation Method at Room Temperature. *Science (80-. )*. **2012**,  
839 28, 555–558.
- 840 38. Al-Janabi, N.; Hill, P.; Torrente-Murciano, L.; Garforth, A.; Gorgojo, P.; Siperstein, F.; Fan, X.  
841 Mapping the Cu-BTC metal-organic framework (HKUST-1) stability envelope in the  
842 presence of water vapour for CO<sub>2</sub> adsorption from flue gases. *Chem. Eng. J.* **2015**, *281*, 669–  
843 677.
- 844 39. Song, Q.; Nataraj, S.K.; Roussanova, M. V.; Tan, J.C.; Hughes, D.J.; Li, W.; Bourgoïn, P.;  
845 Alam, M.A.; Cheetham, A.K.; Al-Muhtaseb, S.A.; et al. Zeolitic imidazolate framework (ZIF-  
846 8) based polymer nanocomposite membranes for gas separation. *Energy Environ. Sci.* **2012**, *5*,  
847 8359.
- 848 40. Pang, S.H.; Han, C.; Sholl, D.S.; Jones, C.W.; Lively, R.P. Facet-specific stability of ZIF-8 in  
849 the presence of acid gases dissolved in aqueous solutions. *Chem. Mater.* **2016**, *28*, 6960–6967.
- 850 41. Yin, H.; Kim, H.; Choi, J.; Yip, A.C.K. Thermal stability of ZIF-8 under oxidative and inert  
851 environments: A practical perspective on using ZIF-8 as a catalyst support. *Chem. Eng. J.*  
852 **2015**, *278*, 293–300.
- 853 42. Jiang, M.; Cao, X.; Liu, P.; Zhang, T.; Zhang, J. ZIF-8@Polyvinylpyrrolidone Nanocomposites  
854 Based N-Doped Porous Carbon for Highly Efficient Oxygen Reduction Reaction in Alkaline  
855 Solution. *J. Electrochem. Soc.* **2016**, *163*, H459–H464.
- 856 43. Zanon, A.; Chaemchuen, S.; Mousavi, B.; Verpoort, F. 1 Zn-doped ZIF-67 as catalyst for the  
857 CO<sub>2</sub> fixation into cyclic carbonates. *J. CO<sub>2</sub> Util.* **2017**, *20*, 282–291.
- 858 44. Wang, S.; Ma, Z.; Du, X.; Zhang, S.; Chen, Z. Lanthanum doping of metal-organic  
859 frameworks-5 and its effect on thermal stability and CO<sub>2</sub> adsorption property. *Mater.*  
860 *Express* **2018**, *8*, 381–387.
- 861 45. Zhou, K.; Mousavi, B.; Luo, Z.; Phatanasri, S.; Chaemchuen, S.; Verpoort, F. Characterization  
862 and properties of Zn/Co zeolitic imidazolate frameworks vs. ZIF-8 and ZIF-67. *J. Mater.*  
863 *Chem. A* **2017**, *5*, 952–957.
- 864 46. Bosch, M.; Zhang, M.; Zhou, H. Increasing the Stability of Metal-Organic Frameworks.  
865 *Adv. in Chem.* **2014**, *10*, 18232–28237.  
866
- 867 47. Giraldo, L.; Barranco, M.B.; Húmpola, P.; Carlos, J.; Piraján, M. the adsorption of phenols  
868 derivatives in aqueous solution. *J. Chem.* **2017**, *8*, 6940–6949.
- 869 48. Zhou, L.; Li, N.; Owens, G.; Chen, Z. Simultaneous removal of mixed contaminants, copper  
870 and norfloxacin, from aqueous solution by ZIF-8. *Chem. Eng. J.* **2019**, *362*, 628–637.
- 871 49. Mao, J.; Ge, M.; Huang, J.; Lai, Y.; Lin, C.; Zhang, K.; Meng, K.; Tang, Y. Constructing  
872 multifunctional MOF@rGO hydro-/aerogels by the self-assembly process for customized  
873 water remediation. *J. Mater. Chem. A* **2017**, *5*, 11873–11881.

- 874 50. Luanwuthi, S.; Krittayavathananon, A.; Srimuk, P.; Sawangphruk, M. In situ synthesis of  
875 permselective zeolitic imidazolate framework-8/graphene oxide composites: rotating disk  
876 electrode and Langmuir adsorption isotherm. *RSC Adv.* **2015**, *5*, 46617–46623.
- 877 51. Biswal, B.P.; Shinde, D.B.; Pillai, V.K.; Banerjee, R. Stabilization of graphene quantum dots  
878 (GQDs) by encapsulation inside zeolitic imidazolate framework nanocrystals for  
879 photoluminescence tuning. *Nanoscale* **2013**, *5*, 10556–10561.
- 880 52. Tanaka, S.; Fujita, K.; Miyake, Y.; Miyamoto, M.; Hasegawa, Y.; Makino, T.; Van Der Perre,  
881 S.; Cousin Saint Remi, J.; Van Assche, T.; Baron, G. V.; et al. Adsorption and Diffusion  
882 Phenomena in Crystal Size Engineered ZIF-8 MOF. *J. Phys. Chem. C* **2015**, *119*, 28430–28439.
- 883 53. Pham, T.T.; Le, L.N.; Nguyen, H.N.; Luong, T.T.K.; Pham, T.N.; Nguyen, H.L.; Nguyen, T.K.  
884 Encapsulating gold nanoparticles in zeolitic imidazolate framework crystal for novel optical  
885 response. *Polyhedron* **2018**, *148*, 171–177.
- 886 54. Goyal, S.; Shaharun, M.S.; Kait, C.F.; Abdullah, B. Effect of monometallic copper on zeolitic  
887 imidazolate framework-8 synthesized by hydrothermal method. *J. Phys. Conf. Ser.* **2018**, *1123*,  
888 0–6.
- 889 55. Zhou, K.; Mousavi, B.; Luo, Z.; Phatanasri, S.; Chaemchuen, S.; Verpoort, F. Characterization  
890 and properties of Zn/Co zeolitic imidazolate frameworks vs. ZIF-8 and ZIF-67. *J. Mater.*  
891 *Chem. A* **2017**, *5*, 952–957.
- 892 56. Li, P.Z.; Wang, X.J.; Liu, J.; Lim, J.S.; Zou, R.; Zhao, Y. A Triazole-Containing Metal-Organic  
893 Framework as a Highly Effective and Substrate Size-Dependent Catalyst for CO<sub>2</sub>  
894 Conversion. *J. Am. Chem. Soc.* **2016**, *138*, 2142–2145.
- 895 57. Abhang, R.M.; Wani, K.S.; Patil, V.S. Synthesis and Characterization of ZIF-8 Filler for  
896 Preparation of Mixed Matrix Membrane. **2015**, *6*, 1276–1280.
- 897 58. Kim, H.U.; Babu, R.; Roshan, R.; Park, D.W. Catalytic performance of metal azolate  
898 frameworks in the solventless synthesis of cyclic carbonates from CO<sub>2</sub> and epoxides. *Appl.*  
899 *Catal. A Gen.* **2017**, *538*, 59–65.
- 900 59. Kim, J.; Kim, S.N.; Jang, H.G.; Seo, G.; Ahn, W.S. CO<sub>2</sub> cycloaddition of styrene oxide over  
901 MOF catalysts. *Appl. Catal. A Gen.* **2013**, *453*, 175–180.
- 902 60. Wang, M.; She, Y.; Zhou, X.; Ji, H. Efficient solvent-free synthesis of chloropropene  
903 carbonate from the coupling reaction of CO<sub>2</sub> and epichlorohydrin catalyzed by magnesium  
904 porphyrins as chlorophyll-like catalysts. *Chinese J. Chem. Eng.* **2011**, *19*, 446–451.
- 905 61. Onyenkeadi, V.; Aboelazayem, O.; Saha, B. Systematic multivariate optimisation of butylene  
906 carbonate synthesis via CO<sub>2</sub> utilisation using graphene-inorganic nanocomposite catalysts.  
907 *Catal. Today* **2019**, *03*, 1–13.
- 908 62. Adeleye, A. I. (Supervisor-Saha. B) Heterogeneous Catalytic Conversion of Carbon Dioxide

- 909 to value Added Chemicals. PhD Thesis, *London South Bank University, London UK*. June, 2015.
- 910 63. Liang, J.; Chen, R.-P.; Wang, X.-Y.; Liu, T.-T.; Wang, X.-S.; Huang, Y.-B.; Cao, R.  
911 Postsynthetic ionization of an imidazole-containing metal–organic framework for the  
912 cycloaddition of carbon dioxide and epoxides. *Chem. Sci.* **2017**, *8*, 1570–1575.
- 913 64. Dhakshinamoorthy, A.; Asiri, A.M.; Garcia, H. Metal-organic frameworks as heterogeneous  
914 catalysts in liquid phase reactions: Why are they so exceptional? *Chim. Oggi/Chemistry Today*  
915 **2015**, *33*, 40–45.
- 916 65. Adeleye, A.I.; Patel, D.; Niyogi, D.; Saha, B. Efficient and greener synthesis of propylene  
917 carbonate from carbon dioxide and propylene oxide. *Ind. Eng. Chem. Res.* **2014**, *53*, 18647–  
918 18657.
- 919 66. Saada, R.; Kellici, S.; Heil, T.; Morgan, D.; Saha, B. Greener synthesis of dimethyl carbonate  
920 using a novel ceria-zirconia oxide/graphene nanocomposite catalyst. *Appl. Catal. B Environ.*  
921 **2015**, *168–169*, 353–362.
- 922 67. Mousavi, B.; Chaemchuen, S.; Phatanasri, S.; Chen, C.; Zeng, C.; Ganguly, R.; Zhuiykov, S.;  
923 Verpoort, F. Selective cyclodimerization of epichlorohydrin to dioxane derivatives over  
924 MOFs. *Arab. J. Chem.* **2017**, *10*, 1878–1888.
- 925 68. Miralda, C.M.; Macías, E.E.; Zhu, M.; Ratnasamy, P.; Carreon, M.A. Zeolitic imidazole  
926 framework-8 catalysts in the conversion of CO<sub>2</sub> to chloropropene carbonate. *ACS Catal.* **2012**,  
927 *2*, 180–183.
- 928 69. Carreon, M.A. Metal organic frameworks as catalysts in the conversion of CO<sub>2</sub>  
929 to cyclic carbonates. *Indian J. Chem. - Sect. A Inorganic, Phys. Theor. Anal. Chem.* **2012**, *51*, 1306–  
930 1314.
- 931 70. Kim, S.H.; Babu, R.; Kim, D.W.; Lee, W.; Park, D.W. Cycloaddition of CO<sub>2</sub> and propylene  
932 oxide by using M(HBTC)(4,4'-bipy)-3DMF (M = Ni, Co, Zn) metal-organic frameworks.  
933 *Cuihua Xuebao/Chinese J. Catal.* **2018**, *39*, 1311–1319.
- 934 71. de Caro, P.; Bandres, M.; Urrutigoity, M.; Cecutti, C.; Thiebaud-Roux, S. Recent progress in  
935 synthesis of glycerol carbonate and evaluation of its plasticizing properties. *Front. Chem.*  
936 **2019**, *7*, 1–13.
- 937 72. Yuan, S.; Zou, L.; Li, H.; Chen, Y.P.; Qin, J.; Zhang, Q.; Lu, W.; Hall, M.B.; Zhou, H.C.  
938 Flexible Zirconium Metal-Organic Frameworks as Bioinspired Switchable Catalysts. *Angew.*  
939 *Chemie - Int. Ed.* **2016**, *55*, 10776–10780.
- 940 73. Bosch, M.; Zhang, M.; Zhou, H.-C. Increasing the Stability of Metal-Organic Frameworks.  
941 *Adv. Chem.* **2014**, 1–8.
- 942 74. Zanon, A.; Chaemchuen, S.; Mousavi, B.; Verpoort, F. 1 Zn-Doped ZIF-67 as Catalyst for the  
943 CO<sub>2</sub> Fixation into Cyclic Carbonates. *J. CO<sub>2</sub> Util.* **2017**, *20* (May), 282–291.